Saturated attitude control of multi-spacecraft systems on SO(3) subject to mixed attitude constraints with arbitrary initial attitude

Zeyu Kang
Shanghai Jiao Tong University, Shanghai, 200240, China

Qiang Shen, Member, IEEE
Shanghai Jiao Tong University, Shanghai, 200240, China

Shufan Wu
Shanghai Jiao Tong University, Shanghai, 200240, China

Christopher J. Damaren
University of Toronto, Toronto, Ontario M3H 5T6, Canada

***Abstract*— In this paper, for multi-spacecraft systems (MSSs) with a directed complete communication topology and a time-varying virtual leader, an adaptive saturated attitude controller is proposed to achieve attitude consensus and attitude tracking under arbitrary initial attitude, mixed attitude constraints, input saturation and external disturbances. Firstly, considering the time-varying desired attitude provided by the virtual leader in a directed complete topology, an MSS attitude error function and an MSS attitude error dynamics based on SO(3) are developed. Next, an effective mixed potential function for the MSS on SO(3) is proposed for the static attitude-forbidden zones, the relative dynamic attitude-forbidden zones and the attitude-mandatory zones. In particular, different from the existing potential functions, the proposed mixed potential function is suitable for arbitrary initial attitude of the spacecraft in MSS, relaxing the restriction on the initial attitude associated with each static and dynamic attitude constraint zones. Then, an adaptive saturated attitude controller is designed to realize attitude consensus and tracking for the MSSs on SO(3) under arbitrary initial attitude, mixed attitude constraints, saturation constraints and external disturbances. Finally, simulation results of an MSS with a time-varying virtual leader are demonstrated to illustrate the efficiency of the proposed attitude controller.**

This work was supported in part by the National Natural Science Foundation of China under Grants with No. 62103275, No. U20B2054, and No. U20B2056. The support provided by China Scholarship Council during a visit of Zeyu Kang to University of Toronto is acknowledged, No. 202106230180.
Corresponding author: Qiang Shen.

Zeyu Kang, Qiang Shen, and Shufan Wu are with the school of Aeronautics and Astronautics, Shanghai Jiao Tong University, Shanghai, 200240, China (e-mail: {kangzeyu, qiangshen, shufan.wu}@sjtu.edu.cn). Christopher J. Damaren is with the Institute for Aerospace Studies, University of Toronto, Toronto, Ontario M3H 5T6, Canada (e-mail: damaren@utias.utoronto.ca).

***Index Terms*— Attitude Consensus; Attitude Tracking; Mixed attitude constraints; Saturated control**

I. Introduction

In recent years, the attitude control of multi-spacecraft systems (MSSs) has attracted tremendous attention. An MSS consists of a number of small spacecraft with low cost, simple structure and shorter development cycles. Through the exchange of information, the spacecraft of MSS can cooperate with each other to complete the space mission to replace the large single spacecraft with complex structure, expensive cost and a longer development cycle. The MSS not only brings modularity to spacecraft design, but also makes the space mission more flexible. At present, MSS has been widely used in the fields of earth observation missions, climate monitoring, deep space exploration, geological survey and spacecraft on-orbit maintenance and service [1]–[3].

Previous studies have developed many attitude representation methods for rigid body attitude control, such as Euler angles, modified Rodriguez parameters (MRPs), unit-quaternion and the special orthogonal group $\mathrm{SO}(3)$ [4]. Euler angles and MRPs have the disadvantage of singularity [5]. Thus, they are not suitable for the needs of spacecraft attitude motion with large-angles. Although the unit-quaternion is a non-Euclidean global parameterization with no singularity, the double coverage of the unit-quaternion results in that two different unit-quaternions represent the same attitude [6]. The attitude model of rigid spacecraft based on $\mathrm{SO}(3)$ can avoid the problems of the above three methods [7], which has attracted extensive research interests. In [8], an adaptive controller on $\mathrm{SO}(3)$ for a rigid spacecraft was designed, which can realize spacecraft attitude redirection under attitude-forbidden constraints. Meanwhile, for the attitude tracking problem of MSS, the distributed strategy has been widely used in missions of MSS to improve the robustness and reduce the communication burden. Each spacecraft of an MSS can only determine its own attitude control command according to its current state and information from neighboring spacecraft [9]–[13]. However, the above works do not take into account the nonlinear input saturation constraint.

Input saturation is a common phenomenon in practical nonlinear control systems, which may lead to the decline of control performance and even the instability of the closed-loop system. In [14], for a class of nonlinear systems with saturation, a robust adaptive controller was proposed by using a Prandtl-Ishlinskii model with play and stop operations. In [15], these operations were further evolved into a dead-zone operator based model of saturation, and the controller was designed using the backstepping method for a group of nonlinear systems with input saturation. For MIMO systems with nonlinear saturated inputs, a robust constrained controller based on dead-zone operation was developed [16]. In [17], the adaptive dynamic surface control of a class of stochastic nonlinear systems with input saturation was studied, where the

saturation nonlinearity was modeled by dead-zone operation and a neural network was used to fit the unknown density function. In [18], the tracking control of marine surface vessels with actuator failure and input saturation was studied, in which the nonlinear saturation was also modeled based on dead-zone operation. For spacecraft attitude control under input saturation control, an adaptive model-free attitude tracking control method was proposed for a rigid spacecraft [19], where a dead-zone based model was used to describe the saturation nonlinearity. In above mentioned works, the input saturation density functions were assumed to be unknown and is treated as a bounded disturbance to be estimated in the controller design. This treatment is obviously conservative and will produce large errors when the extent of saturation is large.

In addition, spacecraft is usually equipped with spaceborne instruments that need to meet multiple attitude constraints in actual space missions [20]. For example, in the process of attitude movement, the spaceborne sensitive equipment (e.g., infrared telescope) needs to avoid direct exposure to the sun or other bright objects, and the communication equipment (e.g., high gain antenna) needs to be kept within the range of the ground station for continuous communication. Currently, the nonlinear optimization method (path planning method [21], [22] or nonlinear model predictive control [23], [24]) and the potential function method are proposed to solve this problem. The method based on nonlinear optimization can obtain the feasible or optimal tracking trajectory of spacecraft attitude. Nevertheless, it may have a complex structure and expensive computational cost, making it not suitable for on-board application. On the contrary, since the attitude controller using potential functions is analytical, it has received extensive attention. In [25], under multiple attitude constraints and angular velocity constraints, the rest-to-rest attitude control of spacecraft was realized by using a quadratic potential function. In [26], the attitude control problem of a single spacecraft with attitude constraints was solved by using the potential function. In [27], using the special orthogonal group $\mathrm{SO}(3)$ attitude parameterization, an adaptive controller based on potential functions was designed to realize the attitude consensus and tracking of MSS under attitude constraints. However, the potential functions in [25]–[27] assume that the initial attitude of the spacecraft must meet the attitude constraints, resulting in limited application range. Moreover, in the MSS, due to the close distance among spacecraft, the bright flame generated by the thrust engines of the neighbor spacecraft will also damage the sensitive spaceborne instruments, which can be considered as a relative dynamic attitude constraint. Due to the complexity caused by this dynamic constraint, there are few studies that take into account this kind of attitude constraint in spacecraft attitude control.

To the best of our knowledge, for MSS with mixed attitude constraints, nonlinear input saturation external disturbances and arbitrary initial attitude, designing an attitude controller on $\mathrm{SO}(3)$ with a time-varying desired attitude provided by the virtual leader spacecraft is still an open problem. To solve this challenging problem, an MSS attitude tracking error model on $\mathrm{SO}(3)$ under a time-varying virtual leader and a directed communication topology (i.e., the information exchange between spacecraft is directional.) is established. Then, the input saturation model based on a dead-zone operation is constructed. For the mixed attitude constraints including static attitude-forbidden zones, the relative dynamic attitude-forbidden zones and the static attitude-mandatory zones, a mixed potential function under the arbitrary initial attitude is proposed. Finally, an adaptive controller is designed to realize consensus and tracking the time-varying desired attitude of MSS on $\mathrm{SO}(3)$ subject to mixed attitude constraints, input saturation and external disturbances. The main contributions of this work are stated as follows:

1) Compared with the existing attitude error function of MSSs on $\mathrm{SO}(3)$ [9], [13], [28], the proposed attitude error function on $\mathrm{SO}(3)$ includes attitude consensus error and time-varying attitude tracking error, making it appliable for a directed communication topology link with a time-varying desired attitude provided by the virtual leader.
2) We design a mixed potential function on $\mathrm{SO}(3)$ accounting for static attitude-forbidden zones, relative dynamic attitude-forbidden zones and static attitude-mandatory zones, which can be effective for arbitrary initial attitude of MSS including that the initial attitude may violate attitude constraints.
3) Considering the mixed attitude constraints, actuator saturation and external disturbances, an adaptive saturated attitude controller is designed for the MSS on $\mathrm{SO}(3)$ to achieve attitude consensus and track the time-varying desired attitude.

The remainder of this paper is organized as follows. The models of the MSS on $\mathrm{SO}(3)$, input saturation and the mixed attitude constraints are constructed in Section II. Problem statements are given in Section III. In Section IV, an MSS attitude tracking error model on $\mathrm{SO}(3)$ under a directed topology is proposed. The potential function for mixed attitude constraints and arbitrary initial attitude of MSS is designed in Section V. Then, an adaptive controller is developed to achieve attitude consensus and track the time-varying desired attitude in Section VI. Simulation results are shown in Section VII. Finally, the Section VIII draws the conclusions.

II. Preliminaries

A. Attitude Kinematics and Dynamics

In this paper, the attitude dynamics of a rigid body is considered. Let $\mathcal{I}$ denote an inertial reference frame and $\mathcal{B}$ denote the body-fixed frame with origin being located at the center of mass. A special group of 3×3 orthogonal matrices used to parameterize attitude is defined as

$$\mathrm{SO}(3)=\left\{\boldsymbol{R}\in\mathbb{R}^{3\times3}\mid\boldsymbol{R}^{\mathrm{T}}\boldsymbol{R}=\boldsymbol{I}_3,\det\boldsymbol{R}=1\right\}. \quad (1)$$

Consider a MSS consisting of N spacecraft. Let $\boldsymbol{R}_i \in \mathrm{SO}(3)$ represent the rotation matrix of the i-th spacecraft from the body frame $\mathcal{B}$ to the inertial reference frame $\mathcal{I}$. The attitude kinematics of the i-th spacecraft can be expressed as [27]

$$\dot{\boldsymbol{R}}_i = \boldsymbol{R}_i \hat{\boldsymbol{\Omega}}_i, \tag{2}$$

where $\boldsymbol{\Omega}_i \in \mathbb{R}^3$ is the inertial angular velocity vector of the i-th spacecraft with respect to an inertial frame $\mathcal{I}$ and expressed in the body-fixed frame $\mathcal{B}$.

In (2), the hat map $\wedge : \mathbb{R}^3 \to \mathfrak{so}(3)$ is used to convert a vector in $\mathbb{R}^3$ to a 3×3 skew-symmetric matrix, which is also the Lie algebra of $\mathrm{SO}(3)$. More explicitly, for a vector $\boldsymbol{x} = [x_1, x_2, x_3]^{\mathrm{T}} \in \mathbb{R}^3$, we have

$$\hat{\boldsymbol{x}} = \begin{bmatrix} 0 & -x_3 & x_2 \\ x_3 & 0 & -x_1 \\ -x_2 & x_1 & 0 \end{bmatrix} \in \mathfrak{so}(3). \tag{3}$$

The attitude of rigid spacecraft can also be expressed as a rotation angle $\theta \leq \pi \in \mathbb{R}$ around a unit vector $\boldsymbol{n} \in \mathbb{R}^2$. This is defined as the exponential mapping [29] of $\mathrm{SO}(3)$, which is given by $\boldsymbol{R} = \exp(\theta, \boldsymbol{n}) \to \mathrm{SO}(3)$ as follows

$$\boldsymbol{R} = \exp(\theta, \boldsymbol{n}) = \boldsymbol{I}_3 + \sin(\theta)\hat{\boldsymbol{n}} + \big(1 - \cos(\theta)\big)\hat{\boldsymbol{n}}^2. \tag{4}$$

The attitude dynamics of the i-th spacecraft is given by [8], [30]

$$\boldsymbol{J}_i \dot{\boldsymbol{\Omega}}_i = -\boldsymbol{\Omega}_i \times \boldsymbol{J}_i \boldsymbol{\Omega}_i + \boldsymbol{w}_i + \boldsymbol{d}_i, \tag{5}$$

where $\boldsymbol{J}_i \in \mathbb{R}^{3\times 3}$, $\boldsymbol{d}_i \in \mathbb{R}^3$ and $\boldsymbol{w}_i = [w_{1,i}, w_{2,i}, w_{3,i}]^{\mathrm{T}} \in \mathbb{R}^3$ denote the symmetric positive definite inertia matrix , the external disturbance and the saturated control torque input of the i-th spacecraft, respectively.

ASSUMPTION 1. *The external disturbance $\boldsymbol{d}_i$ of the i-th spacecraft is bounded by an unknown positive constant $d_{i,\max}$, i.e., $\|\boldsymbol{d}_i\| \leq d_{i,\max}$, $\|\cdot\|$ denotes the Euclidean norm.*

B. The saturated control input model

The nonlinear saturated control input of the i-th spacecraft $\boldsymbol{w}_i = [w_{1,i}, w_{2,i}, w_{3,i}]^{\mathrm{T}} \in \mathbb{R}^3$ in (5) is defined as [16]:

$$w_{m,i} = \mathrm{sat}(u_{m,i}) = \mathrm{sign}(u_{m,i}) \min(u_{\mathrm{sat},m,i}, |u_{m,i}|), \tag{6}$$

where $\mathrm{sign}(\cdot)$ is signum function and $u_{\mathrm{sat},m,i}$ represents the saturation limit of the m-th actuator of the i-th spacecraft with $m = 1, 2, 3$. In order to facilitate the controller design, similar to the method proposed in [14], [31], the nonlinear saturation $\boldsymbol{w}_i = [w_{1,i}, w_{2,i}, w_{3,i}]^{\mathrm{T}}$ can be approximately modeled as $\bar{\boldsymbol{w}}_i = [\bar{w}_{1,i}, \bar{w}_{2,i}, \bar{w}_{3,i}]^{\mathrm{T}}$ by using a dead-zone based model with the following relation:

$$\bar{w}_{m,i} = \rho_{0,m,i} u_{m,i} - \int_0^{K_{m,i}} \rho_{m,i}(k) \mathcal{Z}(k, u_{m,i}) dk, \tag{7}$$

where

1) $\rho_{m,i}(k)$ is considered a unknown density function, which vanishes at a finite horizon $K_{m,i}$ and satisfies $\rho_{m,i}(k) \geq 0, \forall k > 0$.
2) $\rho_{0,m,i} = \int_0^{K_{m,i}} \rho_{m,i}(k) dk$ is a positive unknown constant parameter.

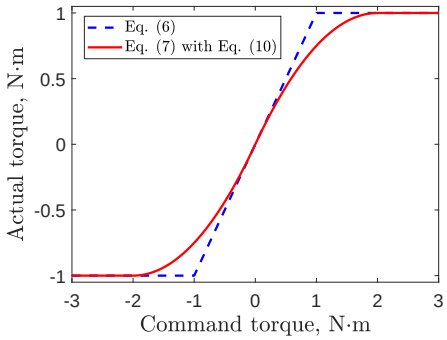

Fig. 1. Comparison of different input saturation operations on the command torque. (The saturation value $u_{\mathrm{sat},m,i}$ is set to ± 1 N·m).

3) The dead-zone operator $\mathcal{Z}(k, u_{m,i})$ is defined by

$$\mathcal{Z}(k, u_{m,i}) = \max\big(u_{m,i} - k, \min(0, u_{m,i} + k)\big). \tag{8}$$

4) The saturated value $u_{\mathrm{sat},m,i}$ can be calculated by

$$u_{\mathrm{sat},m,i} = \lim_{u_{m,i}\to\infty} \bar{w}_{m,i} = \pm \int_0^{K_{m,i}} k \rho_{m,i}(k) dk, \tag{9}$$

which means that $\rho_{m,i}(k)$ can be designed to adapt to the saturation value of the m-th actuator.

In this work, suppose that $\rho_{m,i}(k)$ is designed as

$$\rho_{m,i}(k) = \begin{cases} \frac{1}{K_{m,i}} & k \leq K_{m,i}, \\ 0 & k > K_{m,i}, \end{cases} \tag{10}$$

we can further get $u_{\mathrm{sat},m,i} = \pm \frac{K_{m,i}}{2}$ from (9).

REMARK 1. *In order to illustrate the performance of the dead-zone based saturation operation, we compare the dead-zone based operation (7) with density function (10) and the operation with nonlinear saturation function (6) directly. The actual torque output of the controller command torque under two input saturation operations is shown in Fig. 1. Compared with the nonlinear saturation function (6), the dead-zone based saturation operation (7) with density function (10) makes the process of actual torque reaching or exiting the saturation value smoother without sudden change. In particular, if the dead-zone based operation (7) with density function (10) is adopted, the command torque does not reach the saturation value in the range of $[-2, 2]$ N·m, and the absolute value of the actual torque output is smaller than the operation with nonlinear saturation function (6) in the unsaturated stage. Thus, the saturation operation (7) with density function (10) can reduce the saturation duration.*

Then, the attitude dynamics of the i-th spacecraft can be rewritten as

$$\boldsymbol{J}_i \dot{\boldsymbol{\Omega}}_i = -\boldsymbol{\Omega}_i \times \boldsymbol{J}_i \boldsymbol{\Omega}_i + \bar{\boldsymbol{w}}_i + \boldsymbol{d}_i, \tag{11}$$

with

$$\bar{\boldsymbol{w}}_i = \boldsymbol{\rho}_{0,i} \circ \boldsymbol{u}_i - \mathcal{H}_i \tag{12}$$

where $\boldsymbol{\rho}_{0,i} = [\rho_{0,1,i}, \rho_{0,2,i}, \rho_{0,3,i}]^{\mathrm{T}}$, $\mathcal{H}_i = [h_{1,i}, h_{2,i}, h_{3,i}]^{\mathrm{T}}$ with $h_{m,i} = \int_0^{K_{m,i}} \rho_{m,i}(k) \mathcal{Z}(k, \boldsymbol{u}_{m,i}) dk$ and $m = 1, 2, 3$, $\boldsymbol{u}_i$ represents the controller output to be designed, and the symbol $\circ$ denotes the Hadamard product [32].

C. Graph Theory

The necessary results from algebraic graph theory are introduced in this section. The information communication topology link between the leader spacecraft and the follower N spacecraft can be described by a directed graph $\mathcal{G}=(\mathcal{V},\mathcal{E})$ [27], where $\mathcal{V}=\{1,\cdots,N\}$ denotes the node set and $\mathcal{E}\subset\mathcal{V}\times\mathcal{V}$ is the edge set. The associated adjacency matrix is defined as $\mathcal{A}=[\alpha_{ij}]\in\mathbb{R}^{N\times N}$, where $\alpha_{ij}=1$ if (i,j) is one element of $\mathcal{E}$, i.e., the mode i sends information to the node j, and $\alpha_{ij}=0$ otherwise. Since there is no self-loop for each node in this work, $\alpha_{ii}=0$ holds. The set of in-neighbors of the node i is denoted by $\mathcal{N}_i=\{j\mid(j,i)\in\mathcal{E}\}$. The in-degree matrix of the graph $\mathcal{G}$ is denoted by $\mathcal{D}=\mathrm{diag}\{\mathcal{D}_1,\ldots,\mathcal{D}_N\}$, where $\mathcal{D}_i=\sum_{j\in\mathcal{N}_i}\alpha_{ij}$. The out-neighbors set of the node i is denoted by $\mathcal{O}_i=\{j\mid(i,j)\in\mathcal{E}\}$. The out-degree matrix of the graph $\mathcal{G}$ is denoted by $\mathcal{Q}=\mathrm{diag}\{\mathcal{Q}_1,\ldots,\mathcal{Q}_N\}$, where $\mathcal{Q}_i=\sum_{j\in\mathcal{O}_i}\alpha_{ji}$. Note that $\mathcal{D}_i$ indicates the number of nodes (except the leader) sending information to the node i and $\mathcal{Q}_i$ indicates the number of nodes (except the leader) receiving information from the node i. For a directed complete graph, it satisfies $\mathcal{D}_i=\mathcal{Q}_i=N-1$ for all $i=1,\cdots,N$, i.e., the node i not only receives information from all other nodes j, but also sends information to all other nodes j $(j=1,\cdots,N,j\neq i)$. To describe the information flow from the virtual leader (i.e., node 0) to the followers, the leader adjacency matrix is defined as a diagonal matrix $\mathcal{B}=\mathrm{diag}\{b_1,\ldots,b_N\}$, where $b_i=1$ if the node 0 sends information to node i, and $b_i=0$ otherwise.

D. Mixed Attitude Constraints

Attitude-constrained zones including attitude-forbidden zones and attitude-mandatory zones are considered. The attitude-forbidden zone is defined as an attitude set on which spaceborne sensitive equipment (e.g., infrared telescope) directly exposes to certain bright objects (e.g., bright celestial bodies or bright flames of thrust engines of neighbor spacecraft). The attitude-forbidden zones can be further divided into static and relative dynamic attitude-forbidden zones. On the other hand, the attitude-mandatory zone is an attitude set on which the center pointing of the spaceborne communication equipment keeps in (e.g., the high gain antenna has to point to the ground station to maintain communication). We specify an attitude-mandatory zone for a spaceborne communication equipment.

In this work, the static attitude-forbidden zones, the relative dynamic attitude-forbidden zones and the static attitude-mandatory zones constitute the mixed attitude constraints. Fig. 2 shows an MSS with mixed attitude constraints. For the i-th $(i=1,2,\cdots,N)$ spacecraft, $\boldsymbol{a}_{q,i}$ is the center pointing vector of the q-th $(q=1,2,\cdots,Q)$ spaceborne sensitive equipment (e.g., infrared telescope). In order to meet the static attitude-forbidden constraint, the vector $\boldsymbol{v}_{p,i}$ pointing to the p-th $(p=1,2,\cdots,P)$ bright celestial body must be located outside the field of view of the q-th spaceborne sensitive equipment. Since the direction of p-th bright celestial bodies is static in the inertial frame $\mathcal{I}$, the pointing vector $\boldsymbol{v}_{p,i}$ only changes with the attitude $\boldsymbol{R}_i$ of spacecraft i in the body-fixed frame $\mathcal{B}$, i.e., $\boldsymbol{v}_{p,i}=\boldsymbol{R}_i^{\mathrm{T}}\boldsymbol{v}_{p,i}^I$, where $\boldsymbol{v}_{p,i}^I$ is the vector $\boldsymbol{v}_{p,i}$ expressed in inertial frame $\mathcal{I}$.

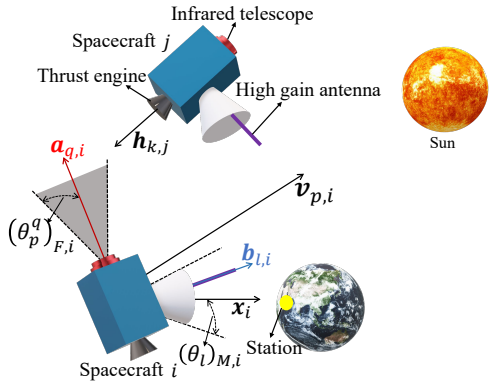

Fig. 2. Multi-spacecraft system with mixed attitude constraints. The vectors in this figure are all unit vectors and all represented in the body-fixed frame $\mathcal{B}$ of the corresponding spacecraft.

Meanwhile, $\boldsymbol{h}_{k,j}$ is the center pointing vector of the k-th $(k=1,2,\cdots,H)$ thrust engine of j-th spacecraft of the MSS, which is the neighbor of i-th spacecraft. In order to satisfy the relative dynamic attitude-forbidden constraint, the direction of vector $\boldsymbol{h}_{k,j}$ must also be outside the field of view of the q-th spaceborne sensitive equipment. Since the $\boldsymbol{h}_{k,j}$ is fixed on the j-th spacecraft, its representation in the body-fixed frame $\mathcal{B}$ of the i-th spacecraft is determined by the relative motion of spacecraft i and spacecraft j, i.e., $\boldsymbol{h}_{k,j}^i=\boldsymbol{R}_i^{\mathrm{T}}\boldsymbol{R}_j\boldsymbol{h}_{k,j}$.

In addition, $\boldsymbol{b}_{l,i}$ is the center-pointing vector of the l-th $(l=1,2,\cdots,L)$ spaceborne communication equipment (e.g., the high gain antenna). In order to meet the attitude-mandatory constraint, the direction of vector $\boldsymbol{b}_{l,i}$ must be within the receiving range of the ground station, and the center direction vector of the ground station is represented by $\boldsymbol{x}_i$. The center direction of the ground station is assumed to be static in the inertial frame $\mathcal{I}$, thus, the vector $\boldsymbol{x}_i$ pointing only changes with the attitude $\boldsymbol{R}_i$ of spacecraft i in the body-fixed frame $\mathcal{B}$, i.e., $\boldsymbol{x}_i=\boldsymbol{R}_i^{\mathrm{T}}\boldsymbol{x}_i^I$, $\boldsymbol{x}_i^I$ is the vector $\boldsymbol{x}_i$ expressed in inertial frame $\mathcal{I}$.

To simulate that different bright objects have different effects on the spaceborne sensitive equipment, their field of views are assumed to be different for different bright objects. Similarly, the receiving range of ground station for different spaceborne communication equipment is also assumed to be different. The field of view of the spaceborne sensitive equipment and the receiving range of the ground station are assumed to be cones. Then, three attitude constraints are defined.

1. *Static Attitude-Forbidden Zone (SFZ)*

The half cone angle of the field of view of the p-th $(p=1,\cdots,P)$ spaceborne sensitive equipment to the q-th $(q=1,\cdots,Q)$ bright celestial body is represented by

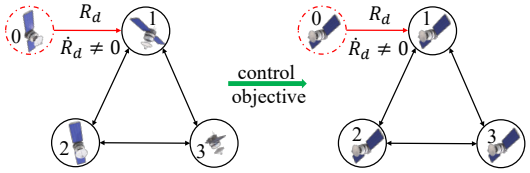

Fig. 3. Control objective: The MSS achieves attitude consensus and tracks the time-varying desired attitude provided by the virtual leader.

$(\theta_p^q)_{F,i} \in [0, \frac{\pi}{2}]$. The corresponding SFZ is expressed as

$$\boldsymbol{a}_{q,i}^{\mathrm{T}} \boldsymbol{v}_{p,i} = \boldsymbol{a}_{q,i}^{\mathrm{T}} \boldsymbol{R}_i^{\mathrm{T}} \boldsymbol{v}_{p,i}^I < \cos\left((\theta_p^q)_{F,i}\right). \tag{13}$$

2. Relative Dynamic Attitude-Forbidden Zone (RFZ)

The half cone angle of the field of view of the p-th ($p = 1, \cdots, P$) spaceborne sensitive equipment to the k-th ($k = 1, \cdots, H$) thrust engine of the j-th neighbor spacecraft is represented by $(\theta_p^{j,k})_{F,i} \in [0, \frac{\pi}{2}]$. The corresponding RFZ is expressed as

$$\boldsymbol{a}_{q,i}^{\mathrm{T}} \boldsymbol{h}_{k,j}^i = \boldsymbol{a}_{q,i}^{\mathrm{T}} \boldsymbol{R}_i^{\mathrm{T}} \boldsymbol{R}_j \boldsymbol{h}_{k,j} < \cos\left((\theta_p^{j,k})_{F,i}\right). \tag{14}$$

3. Static Attitude-Mandatory Zone (SMZ)

The half cone angle of the receiving range of the ground station to the l-th ($l = 1, \cdots, L$) spaceborne communication equipment is expressed by $(\theta_l)_{M,i} \in [0, \frac{\pi}{2}]$. The corresponding SMZ is expressed as

$$\boldsymbol{b}_{l,i}^{\mathrm{T}} \boldsymbol{x}_i = \boldsymbol{b}_{l,i}^{\mathrm{T}} \boldsymbol{R}_i^{\mathrm{T}} \boldsymbol{x}_i^I > \cos\left((\theta_l)_{M,i}\right). \tag{15}$$

ASSUMPTION 2. *The desired attitude $\boldsymbol{R}_d$ of the virtual leader spacecraft provided to the MSS satisfies the mixed attitude constraint model (13), (14) and (15).*

III. Problem Statement

The objective of this paper is to design a saturated attitude control scheme for an MSSs on $\mathrm{SO}(3)$ with mixed attitude constraints, achieving attitude consensus and the attitude tracking of MSSs with arbitrary initial attitude.

In this work, we consider N spacecraft in a directed complete topology, and a virtual leader spacecraft provides the time-varying desired attitude $\boldsymbol{R}_d$ for the MSSs. As shown in Fig. 3, the virtual leader is only connected to the 1-st spacecraft. It is supposed that there is no isolated node in the communication graph, i.e., $\mathcal{N}_i \neq \emptyset \ \forall i$.

In addition, we assume that each spacecraft of the MSSs is equipped with Q sensitive spaceborne equipment to complete the observation missions, L communication spaceborne equipment to communicate with the ground station, H thrust engines and reaction flywheels to change the position and attitude. Meanwhile, the distance between spacecraft in MSS is assumed to be very close, and the thrust engine continues to work to maintain a specific formation configuration (e.g., equilateral triangle configuration). Therefore, the spacecraft needs to avoid the certain bright celestial bodies (e.g., the sun) and the bright flames of the neighbor spacecraft thrust engines to protect the sensitive spaceborne equipment.

This work mainly solves the following three problems:

PROBLEM 1. *[Attitude Error Function and Dynamics on $\mathrm{SO}(3)$ with Time-varying Desired Attitude] Considering the time-varying desired attitude provided by the virtual leader, develop a multi-spacecraft attitude error function and attitude error dynamics on $\mathrm{SO}(3)$ suitable for a directed complete communication topology.*

PROBLEM 2. *[Mixed Potential Function] Considering the static attitude-forbidden zones, the relative dynamic attitude-forbidden zones and the attitude-mandatory zones, propose a mixed potential function for MSSs with arbitrary initial attitude and to avoid reaching the local minimum of the mixed potential function.*

PROBLEM 3. *[Adaptive saturated Continuous Controller] Considering the mixed attitude constraints, saturation constraints and external disturbances, design an adaptive saturation continuous controller to realize attitude consensus and tracking on $\mathrm{SO}(3)$ for MSSs.*

IV. Attitude Error Function and Dynamics on $\mathrm{SO}(3)$ with Time-varying Desired Attitude

Next, we mainly solve Problem 1. The attitude error function and dynamics for an MSSs on $\mathrm{SO}(3)$ with a time-varying desired attitude are developed.

A. Attitude Error Function

Motivated from [8], [30], the attitude error function on $\mathrm{SO}(3)$ of MSSs is given in the following proposition.

PROPOSITION 1. *For the i-th spacecraft, define a attitude error function $\Psi_i \in \mathbb{R}$, an attitude consensus error function $\Psi_{c,i} \in \mathbb{R}$, an attitude tracking error function $\Psi_{t,i} \in \mathbb{R}$, an attitude error vector $\boldsymbol{e}_{\boldsymbol{R},i} \in \mathbb{R}^3$, an attitude consensus error vector $\boldsymbol{e}_{\boldsymbol{R},c,i} \in \mathbb{R}^3$, an attitude tracking error vector $\boldsymbol{e}_{\boldsymbol{R},t,i} \in \mathbb{R}^3$, an angular velocity error vector $\boldsymbol{e}_{\boldsymbol{\Omega},i} \in \mathbb{R}^3$, an angular velocity consistent error vector $\boldsymbol{e}_{\boldsymbol{\Omega},c,i} \in \mathbb{R}^3$ and an angular velocity tracking error vector $\boldsymbol{e}_{\boldsymbol{\Omega},t,i} \in \mathbb{R}^3$ as follows:*

$$\Psi_i = \sum_{j \in \mathcal{N}_i} \Psi_{c,i} + \Psi_{t,i}, \tag{16}$$

$$\Psi_{c,i} = \left(\frac{1}{2} \mathrm{tr}[\boldsymbol{I}_3 - \boldsymbol{R}_j^T \boldsymbol{R}_i]\right), \quad \forall j \in \mathcal{N}_i, \tag{17}$$

$$\Psi_{t,i} = b_i \left(\frac{1}{2} \mathrm{tr}[\boldsymbol{I}_3 - \boldsymbol{R}_d^T \boldsymbol{R}_i]\right), \tag{18}$$

$$\boldsymbol{e}_{\boldsymbol{R},i} = \sum_{j \in \mathcal{N}_i} \boldsymbol{e}_{\boldsymbol{R},c,i} + \boldsymbol{e}_{\boldsymbol{R},t,i}, \tag{19}$$

$$\boldsymbol{e}_{\boldsymbol{R},c,i} = \frac{1}{2} (\boldsymbol{R}_j^T \boldsymbol{R}_i - \boldsymbol{R}_i^T \boldsymbol{R}_j)^\vee, \quad \forall j \in \mathcal{N}_i, \tag{20}$$

$$\boldsymbol{e}_{\boldsymbol{R},t,i} = \frac{1}{2} b_i \left(\boldsymbol{R}_d^T \boldsymbol{R}_i - \boldsymbol{R}_i^T \boldsymbol{R}_d\right)^\vee, \tag{21}$$

$$\boldsymbol{e}_{\boldsymbol{\Omega},c,i} = \boldsymbol{\Omega}_i - \boldsymbol{R}_i^T \boldsymbol{R}_j \boldsymbol{\Omega}_j, \quad \forall j \in \mathcal{N}_i, \tag{22}$$

$$\boldsymbol{e}_{\boldsymbol{\Omega},t,i} = b_i (\boldsymbol{\Omega}_i - \boldsymbol{R}_i^T \boldsymbol{R}_d \boldsymbol{\Omega}_d). \tag{23}$$

Then, we can get the following properties:

1) $\Psi_{c,i}, \Psi_{t,i}$ *and* Ψ_i *are positive semi-definite and their zeros are at* $\boldsymbol{R}_i{=}\boldsymbol{R}_j$, $\boldsymbol{R}_i{=}\boldsymbol{R}_d$ *and* $\boldsymbol{R}_i{=}\boldsymbol{R}_j{=}\boldsymbol{R}_d$.
2) *The left-trivialized derivatives of* $\Psi_{c,i}$, $\Psi_{t,i}$ *and* Ψ_i *with respect to the infinitesimal variation* $\delta\boldsymbol{R}_i = \boldsymbol{R}_i\hat{\boldsymbol{\eta}}$ *for* $\boldsymbol{\eta}\in\mathbb{R}^3$ *are given by*

$$\mathrm{D}_{\boldsymbol{R}_i}(\Psi_{c,i})\cdot\delta\boldsymbol{R}_i = \sum_{j\in\mathcal{N}_i}\boldsymbol{\eta}^{\mathrm{T}}\boldsymbol{e}_{\boldsymbol{R},c,i}, \tag{24}$$

$$\mathrm{D}_{\boldsymbol{R}_i}(\Psi_{t,i})\cdot\delta\boldsymbol{R}_i = \boldsymbol{\eta}^{\mathrm{T}}\boldsymbol{e}_{\boldsymbol{R},t,i}, \tag{25}$$

$$\mathrm{D}_{\boldsymbol{R}_i}(\Psi_{i})\cdot\delta\boldsymbol{R}_i = \boldsymbol{\eta}^{\mathrm{T}}\boldsymbol{e}_{\boldsymbol{R},i}. \tag{26}$$

3) *The vectors* $\boldsymbol{e}_{\boldsymbol{R},c,i}$ *and* $\boldsymbol{e}_{\boldsymbol{R},t,i}$ *are bounded by*

$$0\le\|\boldsymbol{e}_{\boldsymbol{R},c,i}\|\le 1, \tag{27}$$

$$0\le\|\boldsymbol{e}_{\boldsymbol{R},t,i}\|\le b_i. \tag{28}$$

Proof:
According to Rodrigues function, for any $\boldsymbol{Q}=\boldsymbol{R}_j^{\mathrm{T}}\boldsymbol{R}_i\in\mathrm{SO}(3)$, there exists $\boldsymbol{n}\in\mathbb{R}^3$ with $\|\boldsymbol{n}\|\le\pi$ such that

$$\boldsymbol{Q}=\exp(\hat{\boldsymbol{n}})=\boldsymbol{I}_3+\frac{\sin(\|\boldsymbol{n}\|)}{\|\boldsymbol{n}\|}\hat{\boldsymbol{n}}+\frac{1-\cos(\|\boldsymbol{n}\|)}{\|\boldsymbol{n}\|^2}\hat{\boldsymbol{n}}^2. \tag{29}$$

Substituting the foregoing equation into (17), we can get

$$\Psi_{c,i}(\boldsymbol{R}_j\exp(\hat{\boldsymbol{n}}),\boldsymbol{R}_j)=\left(\frac{1}{2}\mathrm{tr}[\boldsymbol{I}_3-\exp(\hat{\boldsymbol{n}})]\right)=1-\cos(\|\boldsymbol{n}\|). \tag{30}$$

Therefore, it is clear that $0\le\Psi_{c,i}\le 2$ and $\Psi_{c,i}=0$ when $\boldsymbol{R}_i=\boldsymbol{R}_j$. Similarly, we can get $0\le\Psi_{t,i}\le 2b_i$ and $\Psi_{t,i}=0$ when $\boldsymbol{R}_i=\boldsymbol{R}_d$ or $b_i=0$ indicating that the i-th spacecraft is not connected to the virtual leader. Because Ψ_i is the addition of $\Psi_{c,i}$ and $\Psi_{t,i}$, Ψ_i is also positive semi-definite and zero at $\boldsymbol{R}_i=\boldsymbol{R}_j=\boldsymbol{R}_d$. These show property 1.

The infinitesimal variation of a rotation matrix can be written as $\delta\boldsymbol{R}=\frac{\mathrm{d}}{\mathrm{d}\epsilon}\big|_{\epsilon=0}\boldsymbol{R}\exp(\epsilon\hat{\boldsymbol{\eta}})=\boldsymbol{R}\hat{\boldsymbol{\eta}}$ for $\boldsymbol{\eta}\in\mathbb{R}^3$ [30]. By leveraging this, the left-trivialized derivative of $\Psi_{c,i}$ with respect to $\boldsymbol{R}_i$ is given by

$$\begin{aligned}\mathrm{D}_{\boldsymbol{R}_i}(\Psi_{c,i})\cdot\delta\boldsymbol{R}_i &= \frac{\mathrm{d}}{\mathrm{d}\epsilon}\Big|_{\epsilon=0}\Psi_{c,i}\big(\boldsymbol{R}_i\exp(\epsilon\hat{\boldsymbol{\eta}}),\boldsymbol{R}_j\big)\\ &= -\frac{1}{2}\mathrm{tr}[\boldsymbol{R}_j^T\boldsymbol{R}_i\hat{\boldsymbol{\eta}}].\end{aligned} \tag{31}$$

Using the fact $\mathrm{tr}[\boldsymbol{R}_j^T\boldsymbol{R}_i\hat{\boldsymbol{\eta}}]=-\boldsymbol{\eta}^{\mathrm{T}}(\boldsymbol{R}_j^T\boldsymbol{R}_i-\boldsymbol{R}_i^T\boldsymbol{R}_j)^\vee$ [30], $\mathrm{D}_{\boldsymbol{R}_i}(\Psi_{c,i})\cdot\delta\boldsymbol{R}_i=\boldsymbol{\eta}^{\mathrm{T}}\boldsymbol{e}_{\boldsymbol{R},c,i}$ is further obtained. Similarly, we can also have $\mathrm{D}_{\boldsymbol{R}_i}(\Psi_{t,i})\cdot\delta\boldsymbol{R}_i=\boldsymbol{\eta}^{\mathrm{T}}\boldsymbol{e}_{\boldsymbol{R},t,i}$ and $\mathrm{D}_{\boldsymbol{R}_i}(\Psi_i)\cdot\delta\boldsymbol{R}_i=\sum_{j\in\mathcal{N}_i}(\boldsymbol{\eta}^{\mathrm{T}}\boldsymbol{e}_{\boldsymbol{R},c,i})+\boldsymbol{\eta}^{\mathrm{T}}\boldsymbol{e}_{\boldsymbol{R},t,i}=\boldsymbol{\eta}^{\mathrm{T}}\boldsymbol{e}_{\boldsymbol{R},i}$. These show property 2. Finally, substituting (29) into (20), we obtain

$$\boldsymbol{e}_{\boldsymbol{R},c,i}=\frac{\sin\|\boldsymbol{n}\|}{\|\boldsymbol{n}\|}\boldsymbol{n}. \tag{32}$$

Thus, $\|\boldsymbol{e}_{\boldsymbol{R},c,i}\|^2=\sin^2\|\boldsymbol{n}\|\le 1$, which implies that $0\le\|\boldsymbol{e}_{\boldsymbol{R},c,i}\|\le 1$. Similarly, we can also obtain $0\le\|\boldsymbol{e}_{\boldsymbol{R},t,i}\|\le b_i$. These show property 3. This completes the proof. ■

REMARK 2. *Proposition 1 defines an attitude consensus error function* $\Psi_{c,i}$ *and an attitude consensus error vector* $\boldsymbol{e}_{\boldsymbol{R},c,i}$ *for attitude consensus requirements, and an attitude tracking error function* $\Psi_{t,i}$ *and an attitude tracking error vector* $\boldsymbol{e}_{\boldsymbol{R},t,i}$ *for desired attitude tracking requirements. The attitude error function (16) includes both attitude consensus error and attitude tracking error, corresponding to the control objective. The minimum point of* Ψ_i *is* $\boldsymbol{R}_i=\boldsymbol{R}_j=\boldsymbol{R}_d$, *which ensures the realization of control objective. In addition, as in* Ψ_i, b_i *indicates whether the* i*-th spacecraft is connected to the virtual leader spacecraft, i.e., it determines whether the attitude tracking requirements need to be considered for the* i*-th spacecraft.*

B. Attitude Error Dynamics

In this section, we derive the attitude error dynamics of the i-th spacecraft. For any desired attitude $\boldsymbol{R}_d^{\mathrm{T}}\boldsymbol{R}_d{=}\boldsymbol{I}_3$. Then, taking the time derivative on both sides results in $\dot{\boldsymbol{R}}_d^{\mathrm{T}}\boldsymbol{R}_d{+}\boldsymbol{R}_d^{\mathrm{T}}\dot{\boldsymbol{R}}_d{=}\boldsymbol{0}$, which further implies

$$\dot{\boldsymbol{R}}_d^{\mathrm{T}}=-\boldsymbol{R}_d^{\mathrm{T}}\dot{\boldsymbol{R}}_d\boldsymbol{R}_d^{\mathrm{T}}. \tag{33}$$

Then, in view of (33), the derivative of $\boldsymbol{R}_d^{\mathrm{T}}\boldsymbol{R}_i$ is

$$\begin{aligned}\boldsymbol{R}_d^{\mathrm{T}}\dot{\boldsymbol{R}}_i{+}\dot{\boldsymbol{R}}_d^{\mathrm{T}}\boldsymbol{R}_i&{=}\boldsymbol{R}_d^{\mathrm{T}}[\boldsymbol{R}_i\hat{\boldsymbol{\Omega}}_i-\boldsymbol{R}_d\hat{\boldsymbol{\Omega}}_d(\boldsymbol{R}_d^{\mathrm{T}}\boldsymbol{R}_i)]\\ &{=}\boldsymbol{R}_d^{\mathrm{T}}\boldsymbol{R}_i[\hat{\boldsymbol{\Omega}}_i-(\boldsymbol{R}_i^{\mathrm{T}}\boldsymbol{R}_d)\hat{\boldsymbol{\Omega}}_d(\boldsymbol{R}_d^{\mathrm{T}}\boldsymbol{R}_i)]\\ &{=}\boldsymbol{R}_d^{\mathrm{T}}\boldsymbol{R}_i(\boldsymbol{\Omega}_i-\boldsymbol{R}_i^{\mathrm{T}}\boldsymbol{R}_d\boldsymbol{\Omega}_d)^\wedge\end{aligned} \tag{34}$$

where the fact $\boldsymbol{R}\hat{\boldsymbol{x}}\boldsymbol{R}^{\mathrm{T}}{=}(\boldsymbol{R}\boldsymbol{x})^\wedge$ for any $\boldsymbol{x}{\in}\mathbb{R}^3$ and $\boldsymbol{R}{\in}\mathrm{SO}(3)$ is used. Following the above derivation, we can get

$$\boldsymbol{R}_j^{\mathrm{T}}\dot{\boldsymbol{R}}_i+\dot{\boldsymbol{R}}_j^{\mathrm{T}}\boldsymbol{R}_i=\boldsymbol{R}_j^{\mathrm{T}}\boldsymbol{R}_i\hat{\boldsymbol{e}}_{\boldsymbol{\Omega},c,i}. \tag{35}$$

Then, it is clear from (17) that

$$\dot{\Psi}_{c,i}=-\frac{1}{2}\mathrm{tr}[\boldsymbol{R}_j^{\mathrm{T}}\boldsymbol{R}_i\hat{\boldsymbol{e}}_{\boldsymbol{\Omega},c,i}]=\boldsymbol{e}_{\boldsymbol{\Omega},c,i}^{\mathrm{T}}\boldsymbol{e}_{\boldsymbol{R},c,i}, \tag{36}$$

the fact $\mathrm{tr}[\boldsymbol{R}_j^T\boldsymbol{R}_i\hat{\boldsymbol{e}}_{\boldsymbol{\Omega},c,i}]{=}{-}\boldsymbol{e}_{\boldsymbol{\Omega},c,i}^{\mathrm{T}}(\boldsymbol{R}_j^T\boldsymbol{R}_i{-}\boldsymbol{R}_i^T\boldsymbol{R}_j)^\vee$ [30] is used. Similarly, by leveraging (34) and (18), we can get

$$\dot{\Psi}_{t,i}=\boldsymbol{e}_{\boldsymbol{\Omega},t,i}^{\mathrm{T}}\boldsymbol{e}_{\boldsymbol{R},t,i}. \tag{37}$$

Obviously, the attitude error dynamics of the i-th spacecraft can be rewritten as

$$\dot{\Psi}_i=\sum_{j\in\mathcal{N}_i}\dot{\Psi}_{c,i}+\dot{\Psi}_{t,i}. \tag{38}$$

Moreover, since the inertia matrix of each spacecraft is positive definite, according to (11), it is trivial to get

$$\dot{\boldsymbol{\Omega}}_i=\boldsymbol{J}_i^{-1}(-\hat{\boldsymbol{\Omega}}_i\boldsymbol{J}_i\boldsymbol{\Omega}_i+\bar{\boldsymbol{w}}_i+\boldsymbol{d}_i). \tag{39}$$

V. Mixed Potential Function

In this section, we mainly solve Problem 2. Based on whether the initial attitude $\boldsymbol{R}_{i,0}$ of the i-th spacecraft meets the mixed attitude constraints (13), (14) or (15), the mixed potential function composed of attractive potential function and repulsive potential function is proposed.

For the static attitude-forbidden zones (SFZ), the static attitude-mandatory zones (SMZ) and the relative dynamic attitude-forbidden zones (DFZ), Φ_i is used to represent the mixed potential function of the i-th spacecraft of the MSSs. The mixed potential function Φ_i that determines whether the attractive potential function is effective or the repulsive potential function is effective according to the initial attitude $\boldsymbol{R}_{i,0}$ is defined as

$$\Phi_i=1+\Phi_{SF,i}+\Phi_{SM,i}+\sum_{j\in\mathcal{N}_i}\Phi_{DF,ij} \tag{40}$$

where

$$\Phi_{SF,i}=\alpha\sum_{p=1}^{P}\sum_{q=1}^{Q}\Bigg(\underbrace{(\gamma_p^q)_{F,i}^1\frac{\left(\boldsymbol{a}_{q,i}^{\mathrm{T}}\boldsymbol{R}_i^{\mathrm{T}}\boldsymbol{v}_{p,i}^I+1\right)^2}{2}}_{\text{Attractive potential function of SFZ}} \underbrace{-(\gamma_p^q)_{F,i}^2\log\Big(\frac{\cos\left((\theta_p^q)_{F,i}\right)-\boldsymbol{a}_{q,i}^{\mathrm{T}}\boldsymbol{R}_i^{\mathrm{T}}\boldsymbol{v}_{p,i}^I}{1+\cos\left((\theta_p^q)_{F,i}\right)}\Big)}_{\text{Repulsive potential function of SFZ}}\Bigg), \tag{41}$$

with

$$\begin{cases}(\gamma_p^q)_{F,i}^1=1,(\gamma_p^q)_{F,i}^2=0 & \text{if } \boldsymbol{a}_{q,i}^{\mathrm{T}}\boldsymbol{R}_{i,0}^{\mathrm{T}}\boldsymbol{v}_{p,i}^I\geq\cos\left((\theta_p^q)_{F,i}\right),\\ (\gamma_p^q)_{F,i}^1=0,(\gamma_p^q)_{F,i}^2=1 & \text{if } \boldsymbol{a}_{q,i}^{\mathrm{T}}\boldsymbol{R}_{i,0}^{\mathrm{T}}\boldsymbol{v}_{p,i}^I<\cos\left((\theta_p^q)_{F,i}\right),\end{cases}$$

$$\Phi_{SM,i}=\lambda\sum_{l=1}^{L}\Bigg(\underbrace{(\gamma_l)_{M,i}^1\frac{\left(1-\boldsymbol{b}_{l,i}^{\mathrm{T}}\boldsymbol{R}_i^{\mathrm{T}}\boldsymbol{x}_i^I\right)^2}{2}}_{\text{Attractive potential function of SMZ}} \underbrace{-(\gamma_l)_{M,i}^2\log\Big(\frac{\boldsymbol{b}_{l,i}^{\mathrm{T}}\boldsymbol{R}_i^{\mathrm{T}}\boldsymbol{x}_i^I-\cos\left((\theta_l)_{M,i}\right)}{1+\cos\left((\theta_l)_{M,i}\right)}\Big)}_{\text{Repulsive potential function of SMZ}}\Bigg), \tag{42}$$

with

$$\begin{cases}(\gamma_l)_{M,i}^1=1,(\gamma_l)_{M,i}^2=0 & \text{if } \boldsymbol{b}_{l,i}^{\mathrm{T}}\boldsymbol{R}_{i,0}^{\mathrm{T}}\boldsymbol{x}_i^I\leq\cos\left((\theta_l)_{M,i}\right),\\ (\gamma_l)_{M,i}^1=0,(\gamma_l)_{M,i}^2=1 & \text{if } \boldsymbol{b}_{l,i}^{\mathrm{T}}\boldsymbol{R}_{i,0}^{\mathrm{T}}\boldsymbol{x}_i^I>\cos\left((\theta_l)_{M,i}\right),\end{cases}$$

$$\Phi_{DF,ij}=\beta\sum_{k=1}^{H}\sum_{q=1}^{Q}\Bigg(\underbrace{(\gamma_p^{j,k})_{F,i}^1\frac{\left(\boldsymbol{a}_{q,i}^{\mathrm{T}}\boldsymbol{R}_i^{\mathrm{T}}\boldsymbol{R}_j\boldsymbol{h}_{k,j}+1\right)^2}{2}}_{\text{Attractive potential function of DFZ}} \underbrace{-(\gamma_p^{j,k})_{F,i}^2\log\Big(\frac{\cos\left((\theta_p^{j,k})_{F,i}\right)-\boldsymbol{a}_{q,i}^{\mathrm{T}}\boldsymbol{R}_i^{\mathrm{T}}\boldsymbol{R}_j\boldsymbol{h}_{k,j}}{1+\cos\left((\theta_p^{j,k})_{F,i}\right)}\Big)}_{\text{Repulsive potential function of DFZ}}\Bigg), \tag{43}$$

with

$$\begin{cases}(\gamma_p^{j,k})_{F,i}^1=1,(\gamma_p^{j,k})_{F,i}^2=0 \text{ if } \boldsymbol{a}_{q,i}^{\mathrm{T}}\boldsymbol{R}_{i,0}^{\mathrm{T}}\boldsymbol{R}_{j,0}\boldsymbol{h}_{k,j}\geq\cos\left((\theta_p^{j,k})_{F,i}\right),\\ (\gamma_p^{j,k})_{F,i}^1=0,(\gamma_p^{j,k})_{F,i}^2=1 \text{ if } \boldsymbol{a}_{q,i}^{\mathrm{T}}\boldsymbol{R}_{i,0}^{\mathrm{T}}\boldsymbol{R}_{j,0}\boldsymbol{h}_{k,j}<\cos\left((\theta_p^{j,k})_{F,i}\right),\end{cases}$$

where α, β and λ are the positive constant weighting parameters for the static attitude-forbidden potential function $\Phi_{SF,i}$, the static attitude-mandatory potential function $\Phi_{SM,i}$ and the relative dynamic attitude-forbidden potential function $\Phi_{DF,ij}$, respectively.

REMARK 3. *Compared with the potential functions in [25]–[27], the proposed potential function Φ_i additionally considers the DFZ. In particular, for the i-th spacecraft in MSSs, when the initial attitude $\boldsymbol{R}_{i,0}$ does not meet the attitude constraints (13), (14) or (15), the attractive potential function works and generates the attractive potential to make the spacecraft quickly satisfy the attitude constraints. (e.g., when the attractive potential function in the static attitude-forbidden potential function $\Phi_{SF,i}$ is effective. The attitude $\boldsymbol{R}_i$ will tend to $\boldsymbol{a}_{q,i}^{\mathrm{T}}\boldsymbol{R}_i^{\mathrm{T}}\boldsymbol{v}_{p,i}^I\to-1=\cos(\pi)$, i.e., use the maximum potential (At present, the angle between $\boldsymbol{a}_{q,i}^{\mathrm{T}}$ and $\boldsymbol{R}_i^{\mathrm{T}}\boldsymbol{v}_{p,i}^I$ is π, and the potential is the largest.) to make the p-th spaceborne sensitive equipment quickly leave the q-th static attitude-forbidden zone). In this case, the sensitive/communication spaceborne equipment is set not to work until the mixed attitude constraints are met. Otherwise, when the initial attitude $\boldsymbol{R}_{i,0}$ satisfies the attitude constraints (13), (14) or (15), the repulsive potential function is effective. When the attitude approaches the edge of the constraint zone (e.g., $\boldsymbol{a}_{q,i}^{\mathrm{T}}\boldsymbol{R}_i^{\mathrm{T}}\boldsymbol{v}_{p,i}^I=\cos((\theta_p^q)_{F,i})$), will make the proposed repulsive potential function of (40) tend to infinity and generate repulsive moment, which will change the attitude of spacecraft i to meet the attitude constraints.*

Then, the time derivative of potential function Φ_i is

$$\begin{aligned}\dot{\Phi}_i=&\dot{\Phi}_{SF,i}+\dot{\Phi}_{SM,i}+\sum_{j\in\mathcal{N}_i}\dot{\Phi}_{DF,ij}\\ =&\boldsymbol{\Omega}_i^{\mathrm{T}}\mathcal{P}_{SF,i}+\boldsymbol{\Omega}_i^{\mathrm{T}}\mathcal{P}_{SM,i}+\sum_{j\in\mathcal{N}_i}(\boldsymbol{e}_{\boldsymbol{\Omega},c,i}^{\mathrm{T}}\mathcal{P}_{DF,ij}),\end{aligned} \tag{44}$$

where

$$\mathcal{P}_{SF,i}=\alpha\sum_{p=1}^{P}\sum_{q=1}^{Q}\Bigg(\Big[-(\gamma_p^q)_{F,i}^1\left(\boldsymbol{a}_{q,i}^{\mathrm{T}}\boldsymbol{R}_i^{\mathrm{T}}\boldsymbol{v}_{p,i}^I+1\right)+(\gamma_p^q)_{F,i}^2\frac{1}{\boldsymbol{a}_{q,i}^{\mathrm{T}}\boldsymbol{R}_i^{\mathrm{T}}\boldsymbol{v}_{p,i}^I-\cos\left((\theta_p^q)_{F,i}\right)}\Big](\boldsymbol{R}_i^{\mathrm{T}}\boldsymbol{v}_{p,i}^I)^{\wedge}\boldsymbol{a}_{q,i}\Bigg),$$

$$\mathcal{P}_{MF,i}=\lambda\sum_{l=1}^{L}\Bigg(\Big[(\gamma_l)_{M,i}^1\left(1-\boldsymbol{b}_{l,i}^{\mathrm{T}}\boldsymbol{R}_i^{\mathrm{T}}\boldsymbol{x}_i^I\right)+(\gamma_l)_{M,i}^2\frac{1}{\boldsymbol{b}_{l,i}^{\mathrm{T}}\boldsymbol{R}_i^{\mathrm{T}}\boldsymbol{x}_i^I-\cos\left((\theta_l)_{M,i}\right)}\Big](\boldsymbol{R}_i^{\mathrm{T}}\boldsymbol{x}_i^I)^{\wedge}\boldsymbol{b}_{l,i}\Bigg),$$

$$\mathcal{P}_{DF,ij}=\beta\sum_{k=1}^{H}\sum_{q=1}^{Q}\Bigg(\Big[-(\gamma_p^{j,k})_{F,i}^1\left(\boldsymbol{a}_{q,i}^{\mathrm{T}}\boldsymbol{R}_i^{\mathrm{T}}\boldsymbol{R}_j\boldsymbol{h}_{k,j}+1\right)+(\gamma_p^{j,k})_{F,i}^2\frac{1}{\boldsymbol{a}_{q,i}^{\mathrm{T}}\boldsymbol{R}_i^{\mathrm{T}}\boldsymbol{R}_j\boldsymbol{h}_{k,j}-\cos\left((\theta_p^{j,k})_{F,i}\right)}\Big](\boldsymbol{R}_i^{\mathrm{T}}\boldsymbol{R}_j\boldsymbol{h}_{k,j})^{\wedge}\boldsymbol{a}_{q,i}\Bigg).$$

Next, we take the static attitude-forbidden potential function $\Phi_{SF,i}$ as an example to derive its derivative with respect to time t in detail. The time derivative of the potential function $\Phi_{SF,i}$ can be computed as

$$\dot{\Phi}_{SF,i}=\alpha\sum_{p=1}^{P}\sum_{q=1}^{Q}\Bigg((\gamma_p^q)_{F,i}^1\left(\boldsymbol{a}_{q,i}^{\mathrm{T}}\boldsymbol{R}_i^{\mathrm{T}}\boldsymbol{v}_{p,i}^I+1\right)\boldsymbol{a}_{q,i}^{\mathrm{T}}\dot{\boldsymbol{R}}_i^{\mathrm{T}}\boldsymbol{v}_{p,i}^I+(\gamma_p^q)_{F,i}^2\frac{\boldsymbol{a}_{q,i}^{\mathrm{T}}\dot{\boldsymbol{R}}_i^{\mathrm{T}}\boldsymbol{v}_{p,i}^I}{\cos\left((\theta_p^q)_{F,i}\right)-\boldsymbol{a}_{q,i}^{\mathrm{T}}\boldsymbol{R}_i^{\mathrm{T}}\boldsymbol{v}_{p,i}^I}\Bigg). \tag{45}$$

According to the attitude kinematics (2), $\dot{\boldsymbol{R}}_i^{\mathrm{T}}=(\boldsymbol{R}_i\hat{\boldsymbol{\Omega}}_i)^{\mathrm{T}}=-\hat{\boldsymbol{\Omega}}_i\boldsymbol{R}_i^{\mathrm{T}}$ can be obtained, where the fact that $\hat{\boldsymbol{\Omega}}_i^{\mathrm{T}}=-\hat{\boldsymbol{\Omega}}_i$ is used. Then, (45) can be rewritten as

$$\dot{\Phi}_{SF,i}=\alpha\sum_{p=1}^{P}\sum_{q=1}^{Q}\Bigg(\Big[-(\gamma_p^q)_{F,i}^1\left(\boldsymbol{a}_{q,i}^{\mathrm{T}}\boldsymbol{R}_i^{\mathrm{T}}\boldsymbol{v}_{p,i}^I+1\right)+(\gamma_p^q)_{F,i}^2\frac{1}{\boldsymbol{a}_{q,i}^{\mathrm{T}}\boldsymbol{R}_i^{\mathrm{T}}\boldsymbol{v}_{p,i}^I-\cos\left((\theta_p^q)_{F,i}\right)}\Big]\boldsymbol{a}_{q,i}^{\mathrm{T}}\hat{\boldsymbol{\Omega}}_i\boldsymbol{R}_i^{\mathrm{T}}\boldsymbol{v}_{p,i}^I\Bigg). \tag{46}$$

Applying the fact [30] $\hat{\boldsymbol{x}}\boldsymbol{y}=-\hat{\boldsymbol{y}}\boldsymbol{x}$ for any $\boldsymbol{x},\boldsymbol{y}\in\mathbb{R}^3$ to the term $\boldsymbol{a}_{q,i}^{\mathrm{T}}\hat{\boldsymbol{\Omega}}_i\boldsymbol{R}_i^{\mathrm{T}}\boldsymbol{v}_{p,i}^I$ yields

$$\boldsymbol{a}_{q,i}^{\mathrm{T}}\hat{\boldsymbol{\Omega}}_i\boldsymbol{R}_i^{\mathrm{T}}\boldsymbol{v}_{p,i}^I=-\boldsymbol{a}_{q,i}^{\mathrm{T}}(\boldsymbol{R}_i^{\mathrm{T}}\boldsymbol{v}_{p,i}^I)^{\wedge}\boldsymbol{\Omega}_i=\boldsymbol{\Omega}_i^{\mathrm{T}}(\boldsymbol{R}_i^{\mathrm{T}}\boldsymbol{v}_{p,i}^I)^{\wedge}\boldsymbol{a}_{q,i}, \tag{47}$$

where the fact that $((\boldsymbol{R}_i^{\mathrm{T}}\boldsymbol{v}_{p,i}^I)^{\wedge})^{\mathrm{T}}=-(\boldsymbol{R}_i^{\mathrm{T}}\boldsymbol{v}_{p,i}^I)^{\wedge}$ is used. Then, substituting (47) into $\dot{\Phi}_{SF,i}$ (46), we can obtain $\dot{\Phi}_{SF,i}=\boldsymbol{\Omega}_i^{\mathrm{T}}\mathcal{P}_{SF,i}$.

Similarly, we can get $\dot{\Phi}_{SM,i}=\boldsymbol{\Omega}_i^{\mathrm{T}}\mathcal{P}_{SM,i}$. In addition, for the relative dynamic attitude-forbidden potential function $\Phi_{DF,ij}$, the difference is that the time derivative of term $\boldsymbol{R}_i^{\mathrm{T}}\boldsymbol{R}_j$ needs to be obtained. Specifically, we have

$$\frac{d\left(\boldsymbol{R}_i^{\mathrm{T}}\boldsymbol{R}_j\right)}{dt}=(\boldsymbol{R}_j^{\mathrm{T}}\boldsymbol{R}_i\hat{\boldsymbol{e}}_{\boldsymbol{\Omega},c,i})^{\mathrm{T}}=-\hat{\boldsymbol{e}}_{\boldsymbol{\Omega},c,i}\boldsymbol{R}_i^{\mathrm{T}}\boldsymbol{R}_j, \quad (48)$$

where the facts (34), (35) and $\hat{\boldsymbol{e}}_{\boldsymbol{\Omega},c,i}^{\mathrm{T}}=-\hat{\boldsymbol{e}}_{\boldsymbol{\Omega},c,i}$ are used. Then, following the same steps above (45)-(47), we can also get $\sum\limits_{j\in\mathcal{N}_i}\dot{\Phi}_{DF,ij}=\sum\limits_{j\in\mathcal{N}_i}(\boldsymbol{e}_{\boldsymbol{\Omega},c,i}^{\mathrm{T}}\mathcal{P}_{DF,ij})$.

PROPOSITION 2. *The mixed potential function in (40) has the following properties:*

1) Φ_i *is positive definite.*
2) $\Phi_i\geq 1$.
3) *The minimum point of* $V_{\boldsymbol{R},i}=\Psi_i\Phi_i$ *is* $\boldsymbol{R}_i=\boldsymbol{R}_j=\boldsymbol{R}_d$.
4) *The left-trivialized derivative of* $V_{\boldsymbol{R},i}$ *with respect to the infinitesimal variation* $\delta\boldsymbol{R}_i=\boldsymbol{R}_i\hat{\boldsymbol{\eta}}$ *for* $\boldsymbol{\eta}\in\mathbb{R}^3$ *is* $\mathrm{D}_{\boldsymbol{R}_i}(V_{\boldsymbol{R},i})\cdot\delta\boldsymbol{R}_i=\boldsymbol{\eta}^{\mathrm{T}}\mathcal{F}_i$, *where*

$$\mathcal{F}_i=\boldsymbol{e}_{\boldsymbol{R},i}\Phi_i+\Psi_i(\mathcal{P}_{SF,i}+\mathcal{P}_{MF,i}+\sum_{j\in\mathcal{N}_i}\mathcal{P}_{DF,ij}). \quad (49)$$

Proof:
It is obvious that the attractive potential functions in $\Phi_{SF,i}$, $\Phi_{SM,i}$, and $\Phi_{DF,ij}$ are positive definite. Meanwhile, in view of the fact that $(\theta_p^q)_{F,i}\in[0,\frac{\pi}{2}]$, $(\theta_p^{j,k})_{F,i}\in[0,\frac{\pi}{2}]$ and $(\theta_l)_{M,i}\in[0,\frac{\pi}{2}]$, $\cos(\theta_p^q)_{F,i}\in[0,1]$, then $\cos(\theta_p^{j,k})_{F,i}\in[0,1]$ and $\cos(\theta_l)_{M,i}\in[0,1]$. According to the mixed attitude constraint zone model (13), (14) and (15), we can obtain

$$\begin{aligned}
0<&\frac{\cos\left((\theta_p^q)_{F,i}\right)-\boldsymbol{a}_{q,i}^{\mathrm{T}}\boldsymbol{R}_i^{\mathrm{T}}\boldsymbol{v}_{p,i}^I}{1+\cos\left((\theta_p^q)_{F,i}\right)}\leq 1,\\
0<&\frac{\cos\left((\theta_p^{j,k})_{F,i}\right)-\boldsymbol{a}_{q,i}^{\mathrm{T}}\boldsymbol{R}_i^{\mathrm{T}}\boldsymbol{R}_j\boldsymbol{h}_{k,j}}{1+\cos\left((\theta_p^{j,k})_{F,i}\right)}\leq 1,\\
0<&\frac{\boldsymbol{b}_{l,i}^{\mathrm{T}}\boldsymbol{R}_i^{\mathrm{T}}\boldsymbol{x}_i^I-\cos\left((\theta_l)_{M,i}\right)}{1+\cos\left((\theta_l)_{M,i}\right)}\leq 1,
\end{aligned} \quad (50)$$

Then, $0\leq-\log(x),\forall x\in(0,1]$. These show that properties 1 and 2 are correct. In addition $V_{\boldsymbol{R},i}=\Psi_i\Phi_i$ is composed of two positive terms. Since $\Phi_i\geq 1$, $V_{\boldsymbol{R},i}=\Psi_i\Phi_i=0$ is equivalent to $\Psi_i=0$, then the minimum point of $V_{\boldsymbol{R},i}$ is the same as that of Ψ_i. These show property 3. Since $V_{\boldsymbol{R},i}=\Psi_i\Phi_i$, we further have

$$\mathrm{D}_{\boldsymbol{R}_i}(V_{\boldsymbol{R},i})\cdot\delta\boldsymbol{R}_i=\left(\mathrm{D}_{\boldsymbol{R}_i}(\Psi_i)\cdot\delta\boldsymbol{R}_i\right)\Phi_i+\Psi_i\left(\mathrm{D}_{\boldsymbol{R}_i}(\Phi_i)\cdot\delta\boldsymbol{R}_i\right), \quad (51)$$

in which the first part can be expanded to

$$\begin{aligned}
\mathrm{D}_{\boldsymbol{R}_i}(\Psi_i)\cdot\delta\boldsymbol{R}_i=&\sum_{j\in\mathcal{N}_i}\left(\frac{\mathrm{d}}{\mathrm{d}\epsilon}\Big|_{\epsilon=0}\Psi_{c,i}\left(\boldsymbol{R}_i(\exp\epsilon\hat{\boldsymbol{\eta}}),\boldsymbol{R}_j\right)\right)\\
&+\frac{\mathrm{d}}{\mathrm{d}\epsilon}\Big|_{\epsilon=0}\Psi_{c,i}\left(\boldsymbol{R}_i(\exp\epsilon\hat{\boldsymbol{\eta}}),\boldsymbol{R}_d\right)\\
=&\sum_{j\in\mathcal{N}_i}\left(\frac{1}{2}\operatorname{tr}[-\boldsymbol{R}_j^T\boldsymbol{R}_i(\exp\epsilon\hat{\boldsymbol{\eta}})\hat{\boldsymbol{\eta}}]\big|_{\epsilon=0}\right)\\
&+b_i\frac{1}{2}\operatorname{tr}[-\boldsymbol{R}_d^T\boldsymbol{R}_i(\exp\epsilon\hat{\boldsymbol{\eta}})\hat{\boldsymbol{\eta}}]\big|_{\epsilon=0}\\
=&-\sum_{j\in\mathcal{N}_i}\left(\frac{1}{2}\operatorname{tr}[\boldsymbol{R}_j^T\boldsymbol{R}_i\hat{\boldsymbol{\eta}}]\right)-b_i\frac{1}{2}\operatorname{tr}[\boldsymbol{R}_d^T\boldsymbol{R}_i\hat{\boldsymbol{\eta}}].
\end{aligned} \quad (52)$$

Applying the fact $\operatorname{tr}[\boldsymbol{A}\hat{\boldsymbol{x}}]=-\boldsymbol{x}^{\mathrm{T}}\left(\boldsymbol{A}-\boldsymbol{A}^{\mathrm{T}}\right)^{\vee}$ from [30] for any $\boldsymbol{x}\in\mathbb{R}^3$, $\boldsymbol{A}\in\mathbb{R}^{3\times3}$, we further obtain

$$\begin{aligned}
\mathrm{D}_{\boldsymbol{R}_i}(\Psi_i)\cdot\delta\boldsymbol{R}_i=&\sum_{j\in\mathcal{N}_i}\left(\frac{1}{2}\boldsymbol{\eta}^{\mathrm{T}}\left(\boldsymbol{R}_j^T\boldsymbol{R}_i-\boldsymbol{R}_i^T\boldsymbol{R}_j\right)^{\vee}\right)\\
&-b_i\frac{1}{2}\boldsymbol{\eta}^{\mathrm{T}}\left(\boldsymbol{R}_d^T\boldsymbol{R}_i-\boldsymbol{R}_i^T\boldsymbol{R}_d\right)^{\vee}\\
=&\sum_{j\in\mathcal{N}_i}(\boldsymbol{\eta}^{\mathrm{T}}\boldsymbol{e}_{\boldsymbol{R},c,i})+\boldsymbol{\eta}^{\mathrm{T}}\boldsymbol{e}_{\boldsymbol{R},t,i}=\boldsymbol{\eta}^{\mathrm{T}}\boldsymbol{e}_{\boldsymbol{R},i}.
\end{aligned} \quad (53)$$

Therefore, the first part can be written as

$$\left(\mathrm{D}_{\boldsymbol{R}_i}(\Psi_i)\cdot\delta\boldsymbol{R}_i\right)\Phi_i=\boldsymbol{\eta}^{\mathrm{T}}\boldsymbol{e}_{\boldsymbol{R},i}\Phi_i. \quad (54)$$

For the second part of (51), we have

$$\begin{aligned}
\mathrm{D}_{\boldsymbol{R}_i}(\Phi_i)\cdot\delta\boldsymbol{R}_i=&\frac{\mathrm{d}}{\mathrm{d}\epsilon}\Big|_{\epsilon=0}\Phi_{SF,i}\left(\boldsymbol{R}_i\exp(\epsilon\hat{\boldsymbol{\eta}})\right)\\
&+\frac{\mathrm{d}}{\mathrm{d}\epsilon}\Big|_{\epsilon=0}\Phi_{SM,i}\left(\boldsymbol{R}_i\exp(\epsilon\hat{\boldsymbol{\eta}})\right)\\
&+\sum_{j\in\mathcal{N}_i}\left(\frac{\mathrm{d}}{\mathrm{d}\epsilon}\Big|_{\epsilon=0}\Phi_{DF,ij}\left(\boldsymbol{R}_i\exp(\epsilon\hat{\boldsymbol{\eta}})\right)\right).
\end{aligned} \quad (55)$$

Taking the first term in (55) as an example, we can obtain

$$\begin{aligned}
&\frac{\mathrm{d}}{\mathrm{d}\epsilon}\Big|_{\epsilon=0}\Phi_{SF,i}\left(\boldsymbol{R}_i\exp(\epsilon\hat{\boldsymbol{\eta}})\right)\\
=&\alpha\sum_{p=1}^{P}\sum_{q=1}^{Q}\Bigg(-(\gamma_p^q)_{F,i}^1\left(\boldsymbol{a}_{q,i}^{\mathrm{T}}\boldsymbol{R}_i^{\mathrm{T}}\boldsymbol{v}_{p,i}^I+1\right)\boldsymbol{a}_{q,i}^{\mathrm{T}}\hat{\boldsymbol{\eta}}\boldsymbol{R}_i^{\mathrm{T}}\boldsymbol{v}_{p,i}^I\\
&+(\gamma_p^q)_{F,i}^2\frac{\boldsymbol{a}_{q,i}^{\mathrm{T}}\hat{\boldsymbol{\eta}}\boldsymbol{R}_i^{\mathrm{T}}\boldsymbol{v}_{p,i}^I}{\boldsymbol{a}_{q,i}^{\mathrm{T}}\boldsymbol{R}_i^{\mathrm{T}}\boldsymbol{v}_{p,i}^I-\cos\left((\theta_p^q)_{F,i}\right)}\Bigg)=\boldsymbol{\eta}^{\mathrm{T}}\mathcal{P}_{SF,i},
\end{aligned} \quad (56)$$

where the fact [30] $\hat{\boldsymbol{x}}\boldsymbol{y}=-\hat{\boldsymbol{y}}\boldsymbol{x}$ for any $\boldsymbol{x},\boldsymbol{y}\in\mathbb{R}^3$ is used. For the second and the third terms in (55), we have

$$\begin{aligned}
&\frac{\mathrm{d}}{\mathrm{d}\epsilon}\Big|_{\epsilon=0}\Phi_{SM,i}\left(\boldsymbol{R}_i\exp(\epsilon\hat{\boldsymbol{\eta}})\right)=\boldsymbol{\eta}^{\mathrm{T}}\mathcal{P}_{MF,i}\\
&\sum_{j\in\mathcal{N}_i}\left(\frac{\mathrm{d}}{\mathrm{d}\epsilon}\Big|_{\epsilon=0}\Phi_{DF,ij}\left(\boldsymbol{R}_i\exp(\epsilon\hat{\boldsymbol{\eta}})\right)\right)=\boldsymbol{\eta}^{\mathrm{T}}\sum_{j\in\mathcal{N}_i}\mathcal{P}_{DF,ij}
\end{aligned}$$

Therefore, the second part in (51) can be written as $\Psi_i\left(\mathrm{D}_{\boldsymbol{R}_i}(\Phi_i)\cdot\delta\boldsymbol{R}_i\right)=\Psi_i\boldsymbol{\eta}^{\mathrm{T}}\left(\mathcal{P}_{SF,i}+\mathcal{P}_{MF,i}+\sum\limits_{j\in\mathcal{N}_i}\mathcal{P}_{DF,ij}\right)$. Then, taking into account (54), it is clear that

$$\begin{aligned}
\mathrm{D}_{\boldsymbol{R}_i}(V_{\boldsymbol{R},i})\cdot\delta\boldsymbol{R}_i=&\boldsymbol{\eta}^{\mathrm{T}}\boldsymbol{e}_{\boldsymbol{R},i}\Phi_i\\
&+\Psi_i\boldsymbol{\eta}^{\mathrm{T}}\left(\mathcal{P}_{SF,i}+\mathcal{P}_{MF,i}+\sum_{j\in\mathcal{N}_i}\mathcal{P}_{DF,ij}\right).
\end{aligned} \quad (57)$$

Since both $\Psi_i\in\mathbb{R}$ and $\Phi_i\in\mathbb{R}$, we eventually obtain

$$\mathrm{D}_{\boldsymbol{R}_i}=\boldsymbol{\eta}^{\mathrm{T}}\mathcal{F}_i. \quad (58)$$

These show property 4. ■

REMARK 4. *The property* 3 *of the proposition 2 shows that the system does not fall into the local minimum, since the minimum value of* Ψ_i *is not changed, i.e., the spacecraft attitude finally converges to the desired attitude* $\boldsymbol{R}_d$. *Therefore, in Assumption 2, only the attitude of the virtual leader spacecraft is reasonably limited, and the initial attitude* $\boldsymbol{R}_{i,0}$ *of the* i*-spacecraft is not limited.*

VI. Adaptive Saturated Continuous Controller Design

In this section, we solve Problem 3. An adaptive saturated continuous controller is designed to realize attitude consensus and tracking for the MSSs on SO(3) despite the mixed attitude constraints and saturation constraints.

In practical applications, the unknown parameters $\rho_{0,m,i}$, and $\rho_{m,i}$ in (11) are upper bounded by known scalar constants, thus their estimation can also be limited to a bounded convex set with known bounds [33]. Meanwhile, considering the upper-bounded unknown disturbances $d_{i,\max}$ together (cf. Assumption 1), the following relationship is defined:

$$(\Gamma_{1,i},\Gamma_{2,i},\Gamma_{3,i}) \triangleq (\boldsymbol{\chi}_{\rho_0,i},\boldsymbol{\rho}_i,d_{\max}) \tag{59}$$

where $\boldsymbol{\chi}_{\rho_0,i}=[\frac{1}{\rho_{0,1,i}},\frac{1}{\rho_{0,2,i}},\frac{1}{\rho_{0,3,i}}]^{\mathrm{T}}$, $\boldsymbol{\rho}_i=[\rho_{1,i},\rho_{2,i},\rho_{3,i}]^{\mathrm{T}}$. The estimated values corresponding to (59) are defined as

$$(\hat{\Gamma}_{1,i},\hat{\Gamma}_{2,i},\hat{\Gamma}_{3,i}) \triangleq (\hat{\boldsymbol{\chi}}_{\rho_0,i},\hat{\boldsymbol{\rho}}_i,\hat{d}_{\max}). \tag{60}$$

Then, we define convex sets for $\Gamma_{v,i}$ and $\hat{\Gamma}_{v,i}$ as

$$\begin{aligned}\Pi_{\Gamma_{v,i}} &\triangleq \{\Gamma_{v,i}\in\mathbb{R}^n \mid \Gamma_{v,i}^{\mathrm{T}}\Gamma_{v,i}\le\epsilon_{v,i}\}\\ \Pi_{\hat{\Gamma}_{v,i}} &\triangleq \{\hat{\Gamma}_{v,i}\in\mathbb{R}^n \mid \hat{\Gamma}_{v,i}^{\mathrm{T}}\hat{\Gamma}_{v,i}<\epsilon_{v,i}+\delta_{v,i}\}\end{aligned} \tag{61}$$

where $\epsilon_{v,i}>0$ is the upper bound for $\Gamma_{v,i}$, and $\delta_{v,i}>0$ is a small constant, $v\in\{1,2,3\}$, and superscript n represents the dimension of $\Gamma_{v,i}$. Then, the smooth projection for $\Gamma_{v,i}$ is defined as

$$\dot{\hat{\Gamma}}_{v,i}=\mathrm{Proj}(\hat{\Gamma}_{v,i},\Upsilon_{v,i}) \tag{62}$$

where $\mathrm{Proj}(\hat{\Gamma}_{v,i},\Upsilon_{v,i})\triangleq$

$$\begin{cases}\eta_v\Upsilon_{v,i} & \text{if}\|\hat{\Gamma}_{v,i}\|^2<\epsilon_{v,i}\text{ or}\\ & \text{if}\|\hat{\Gamma}_{v,i}\|^2\ge\epsilon_{v,i}\text{ and}\,\mathcal{W}<0\\ \eta_v\Big(\Upsilon_{v,i}-\frac{(\|\hat{\Gamma}_{v,i}\|^2-\epsilon_{v,i})\mathcal{W}}{\delta_{v,i}\|\hat{\Gamma}_{v,i}\|^2}\hat{\Gamma}_{v,i}\Big) & \text{if}\|\hat{\Gamma}_{v,i}\|^2\ge\epsilon_{v,i}\text{ and}\,\mathcal{W}\ge0\end{cases}$$

where $\mathcal{W}=\Upsilon_{v,i}^{\mathrm{T}}\hat{\Gamma}_{v,i}$ and η_v is a positive constant.

$$\Upsilon_{1,i}\triangleq-\boldsymbol{\Omega}_i\circ\bar{\boldsymbol{u}}_i,\ \Upsilon_{2,i}\triangleq-\boldsymbol{\Omega}_i\circ\mathcal{Z}(r,\boldsymbol{u}_i),\ \Upsilon_{3,i}\triangleq\|\boldsymbol{\Omega}_i\|. \tag{63}$$

Remark 5. *In practical application, the values of $\epsilon_{v,i}$ and $\delta_{v,i}$ can be set according to experience to avoid that the estimation of unknown parameters is not conform to their physical meaning. If the initial estimate of the unknown parameter $\hat{\Gamma}_{v,i}$ satisfies $\hat{\Gamma}_{v,i}^{\mathrm{T}}(0)\hat{\Gamma}_{v,i}(0)<\epsilon_{v,i}+\delta_{v,i}$, then we can limit the estimate of $\hat{\Gamma}_{v,i}$ to a bounded range by the smooth projection $\dot{\hat{\Gamma}}_{v,i}=\mathrm{Proj}(\hat{\Gamma}_{v,i},\Upsilon_{v,i})$.*

Then, in light of attitude error function (16), error dynamics (39) on SO(3) and mixed potential function (40), an adaptive attitude controller is designed as

$$\boldsymbol{u}_i=\hat{\boldsymbol{\chi}}_{\rho_0,i}\circ\bar{\boldsymbol{u}}_i=\hat{\boldsymbol{\chi}}_{\rho_0,i}\circ(\boldsymbol{u}_i^0+\hat{\mathcal{H}}_i), \tag{64}$$

where $\boldsymbol{u}_i^0$ is a virtual controller, and

$$\begin{aligned}\boldsymbol{u}_i^0=&-k_1\Psi_i\mathcal{S}_{1,i}-k_2\|\boldsymbol{e}_{\boldsymbol{\Omega},i}\|\mathcal{S}_{2,i}-k_3\boldsymbol{e}_{\boldsymbol{\Omega},i}\\&-k_4\mathcal{F}_i+k_4\mathcal{M}_i\mathcal{S}_{3,i}-\hat{d}_{i,\max}\mathcal{S}_{4,i}\end{aligned} \tag{65}$$

with $\mathcal{S}_{1,i}=\frac{\boldsymbol{\Omega}_i}{\|\boldsymbol{\Omega}_i\|^2+\kappa_{1,i}^2}$, $\mathcal{S}_{2,i}=\frac{\boldsymbol{\Omega}_i}{\|\boldsymbol{\Omega}_i\|+\kappa_{2,i}^2}$, $\mathcal{S}_{3,i}=\frac{\boldsymbol{\Omega}_i}{\|\boldsymbol{\Omega}_i\|^2+\kappa_{3,i}^2}$, $\mathcal{S}_{4,i}=\frac{\boldsymbol{\Omega}_i}{\|\boldsymbol{\Omega}_i\|+\kappa_{4,i}^2}$, where $\kappa_{1,i},\kappa_{2,i},\kappa_{3,i},\kappa_{4,i}$ are adaptive parameters to be given later, $\mathcal{M}_i=\Psi_i\sum_{j\in\mathcal{N}_i}\big((\boldsymbol{R}_i^T\boldsymbol{R}_j\boldsymbol{\Omega}_j)^{\mathrm{T}}\mathcal{P}_{DF,ij}\big)+\Phi_i\sum_{j\in\mathcal{N}_i}\big((\boldsymbol{R}_i^T\boldsymbol{R}_j\boldsymbol{\Omega}_j)^{\mathrm{T}}\boldsymbol{e}_{\boldsymbol{R},c,i}\big)+\Phi_i\big(b_i(\boldsymbol{R}_i^T\boldsymbol{R}_d\boldsymbol{\Omega}_d)^{\mathrm{T}}\boldsymbol{e}_{\boldsymbol{R},t,i}\big)$, k_1, k_2, k_3 and k_4 are positive constants. In addition, $\hat{\mathcal{H}}_i=[\hat{h}_{1,i},\hat{h}_{2,i},\hat{h}_{3,i}]^{\mathrm{T}}$, and $\hat{h}_{m,i}=\int_0^{K_{m,i}}\hat{\rho}_{m,i}(k)\mathcal{Z}(k,u_{m,i})dk$, $m=1,2,3$. The updating laws for parameters $\boldsymbol{\chi}_{\rho_0,i}$, $\boldsymbol{\rho}_i$, $d_{\max}$, $\kappa_{1,i}$, $\kappa_{2,i}$, $\kappa_{3,i}$, $\kappa_{4,i}$ are proposed as

$$\begin{cases}\dot{\hat{\boldsymbol{\chi}}}_{\rho_0,i}=\mathrm{Proj}(\hat{\boldsymbol{\chi}}_{\rho_0,i},\Upsilon_{1,i}),\dot{\hat{\boldsymbol{\rho}}}_i=\mathrm{Proj}(\hat{\boldsymbol{\rho}}_i,\Upsilon_{2,i}),\\ \dot{\hat{d}}_{i,\max}=\mathrm{Proj}(\hat{d}_{i,\max},\Upsilon_{3,i}),\dot{\kappa}_{1,i}=-\frac{\mu_1\kappa_{1,i}}{\|\boldsymbol{\Omega}_i\|^2+\kappa_{1,i}^2}k_1\Psi_i,\\ \dot{\kappa}_{2,i}=-\frac{\mu_2\kappa_{2,i}}{\|\boldsymbol{\Omega}_i\|+\kappa_{2,i}^2}k_2\|\boldsymbol{\Omega}_i\|\|\boldsymbol{e}_{\boldsymbol{\Omega},i}\|,\\ \dot{\kappa}_{3,i}=\frac{\mu_3\kappa_{3,i}}{\|\boldsymbol{\Omega}_i\|^2+\kappa_{3,i}^2}k_4\mathcal{M}_i,\dot{\kappa}_{4,i}=-\frac{\mu_4\kappa_{4,i}}{\|\boldsymbol{\Omega}_i\|+\kappa_{4,i}^2}\|\boldsymbol{\Omega}_i\|\hat{d}_{i,\max},\end{cases} \tag{66}$$

where μ_1,μ_2,μ_3 and μ_4 are positive constants.

Then, according to (12), the proposed adaptive saturated attitude controller with the dead-zone input saturation operation can be expressed as

$$\bar{\boldsymbol{w}}_i=\boldsymbol{\rho}_{0,i}\circ\hat{\boldsymbol{\chi}}_{\rho_0,i}\circ\bar{\boldsymbol{u}}_i-\mathcal{H}_i=\boldsymbol{\rho}_{0,i}\circ\hat{\boldsymbol{\chi}}_{\rho_0,i}\circ(\boldsymbol{u}_i^0+\hat{\mathcal{H}}_i)-\mathcal{H}_i. \tag{67}$$

Using the proposed adaptive saturated attitude controller in (67) with the adaptive law (66), the stability of the MSSs is summarized in the following theorem.

Theorem 1. *For the attitude error kinematics and dynamics on SO(3) represented by (16) and (39), the proposed adaptive saturated attitude controller (67) with the adaptive law (66) and $k_2\ge k_3>0$ ensures that $\lim_{t\to\infty}\boldsymbol{R}_i=\boldsymbol{R}_j=\boldsymbol{R}_d$ and $\lim_{t\to\infty}\boldsymbol{\Omega}_i=\boldsymbol{\Omega}_j=\boldsymbol{\Omega}_d$, i.e., the proposed adaptive saturated attitude continuous controller (67) can achieve consensus and tracking of time-varying virtual attitude commands of MSSs despite the mixed attitude constraints, input saturation and external disturbances.*

Proof:
Consider the following Lyapunov candidate function:

$$\begin{aligned}V=\sum_{i=1}^{N}\big(&\frac{1}{2}\boldsymbol{\Omega}_i^{\mathrm{T}}\boldsymbol{J}_i\boldsymbol{\Omega}_i+k_4V_{\boldsymbol{R},i}+V_{\boldsymbol{\chi},i}+V_{\boldsymbol{\rho},i}+V_{\boldsymbol{d}_{i,\max}}\\&+V_{\kappa_{1,i}}+V_{\kappa_{2,i}}+V_{\kappa_{3,i}}+V_{\kappa_{4,i}}\big),\end{aligned} \tag{68}$$

where $V_{\boldsymbol{\chi},i}=\frac{1}{2\eta_1}(\boldsymbol{\rho}_{0,i}\circ\tilde{\boldsymbol{\chi}}_{\rho_0,i})^{\mathrm{T}}\tilde{\boldsymbol{\chi}}_{\rho_0,i}$, $V_{\boldsymbol{d}_{i,\max}}=\frac{1}{2\eta_3}\tilde{d}_{i,\max}^2$, $V_{\boldsymbol{\rho},i}=\frac{1}{2\eta_2}\sum_{m=1}^{3}\int_0^{K_{m,i}}\tilde{\rho}_{m,i}^2dk$, $V_{\kappa_{1,i}}=\frac{1}{2\mu_1}\kappa_{1,i}^2$, $V_{\kappa_{2,i}}=\frac{1}{2\mu_2}\kappa_{2,i}^2$, $V_{\kappa_{3,i}}=\frac{1}{2\mu_3}\kappa_{3,i}^2$ and $V_{\kappa_{4,i}}=\frac{1}{2\mu_4}\kappa_{4,i}^2$ with $\tilde{\boldsymbol{\chi}}_{\rho_0,i}=\boldsymbol{\chi}_{\rho_0,i}-\hat{\boldsymbol{\chi}}_{\rho_0,i}$, $\tilde{\rho}_{m,i}=\rho_{m,i}-\hat{\rho}_{m,i}$ and $\tilde{d}_{i,\max}=d_{i,\max}-\hat{d}_{i,\max}$.

The proposed adaptive saturated attitude controller in (67) can be rewritten as

$$\begin{aligned}\bar{\boldsymbol{w}}_i&=\boldsymbol{\rho}_{0,i}\circ\hat{\boldsymbol{\chi}}_{\rho_0,i}\circ\bar{\boldsymbol{u}}_i-\mathcal{H}_i=\boldsymbol{\rho}_{0,i}\circ(\boldsymbol{\chi}_{\rho_0,i}-\tilde{\boldsymbol{\chi}}_{\rho_0,i})\circ\bar{\boldsymbol{u}}_i-\mathcal{H}_i\\&=\boldsymbol{u}_i^0-\boldsymbol{\rho}_{0,i}\circ\tilde{\boldsymbol{\chi}}_{\rho_0,i}\circ\bar{\boldsymbol{u}}_i-(\mathcal{H}_i-\hat{\mathcal{H}}_i).\end{aligned} \tag{69}$$

Then, substituting (11) and the proposed controller (69) into the time derivative of V yields

$$\begin{aligned}\dot{V} \leq \sum_{i=1}^{N} \Big(& -k_1\Psi_i - (k_2-k_3)\|\boldsymbol{\Omega}_i\|\|\boldsymbol{e}_{\boldsymbol{\Omega},i}\| \\ & - \boldsymbol{\Omega}_i^{\mathrm{T}}(\boldsymbol{\rho}_{0,i}\circ\tilde{\boldsymbol{\chi}}_{\rho_0,i}\circ\bar{\boldsymbol{u}}_i) + \tilde{d}_{i,\max}\|\boldsymbol{\Omega}_i\| \\ & - \boldsymbol{\Omega}_i^{\mathrm{T}}(\mathcal{H}_i - \hat{\mathcal{H}}_i) - \frac{1}{\eta_1}(\boldsymbol{\rho}_{0,i}\circ\tilde{\boldsymbol{\chi}}_{\rho_0,i})^{\mathrm{T}}\dot{\hat{\boldsymbol{\chi}}}_{\rho_0,i} \\ & - \frac{1}{\eta_2}\sum_{m=1}^{3}\int_0^{K_{m,i}} \tilde{\rho}_{m,i}\dot{\hat{\rho}}_{m,i}dk - \frac{1}{\eta_3}\tilde{d}_{i,\max}\dot{\hat{d}}_{i,\max}\Big),\end{aligned}$$

where the following facts are sued:

$$\begin{aligned} -k_1\boldsymbol{\Omega}_i^{\mathrm{T}}\Psi_i\mathcal{S}_{1,i} + \frac{1}{\mu_1}\kappa_{1,i}\dot{\kappa}_{1,i} &= -k_1\Psi_i \\ -k_2\boldsymbol{\Omega}_i^{\mathrm{T}}\|\boldsymbol{e}_{\boldsymbol{\Omega},i}\|\mathcal{S}_{2,i} + \frac{1}{\mu_2}\kappa_{2,i}\dot{\kappa}_{2,i} &= -k_2\|\boldsymbol{\Omega}_i\|\|\boldsymbol{e}_{\boldsymbol{\Omega},i}\| \\ k_4\boldsymbol{\Omega}_i^{\mathrm{T}}\mathcal{M}_i\mathcal{S}_{3,i} + \frac{1}{\mu_3}\kappa_{3,i}\dot{\kappa}_{3,i} &= k_4\mathcal{M}_i \\ -\boldsymbol{\Omega}_i^{\mathrm{T}}\hat{d}_{i,\max}\mathcal{S}_{4,i} + \frac{1}{\mu_4}\kappa_{4,i}\dot{\kappa}_{4,i} &= -\hat{d}_{i,\max}\|\boldsymbol{\Omega}_i\| \\ k_4\dot{V}_{\boldsymbol{R}_i} = k_4(\dot{\Psi}_i\Phi_i + \Psi_i\dot{\Phi}_i) &= k_4\boldsymbol{\Omega}_i^{\mathrm{T}}\mathcal{F}_i - k_4\mathcal{M}_i. \end{aligned}$$

Then, we have $\dot{V}\leq\sum_{i=1}^{N}\Big(-k_1\Psi_i-(k_2-k_3)\|\boldsymbol{\Omega}_i\|\|\boldsymbol{e}_{\boldsymbol{\Omega},i}\|+\mathcal{C}_{1,i}+\mathcal{C}_{2,i}+\mathcal{C}_{3,i}\Big)$, where

$$\begin{aligned} \mathcal{C}_{1,i} &= -\frac{1}{\eta_1}(\boldsymbol{\rho}_{0,i}\circ\tilde{\boldsymbol{\chi}}_{\rho_0,i})^{\mathrm{T}}(\dot{\hat{\boldsymbol{\chi}}}_{\rho_0,i} + \eta_1\boldsymbol{\Omega}_i\circ\bar{\boldsymbol{u}}_i), \\ \mathcal{C}_{2,i} &= -\frac{1}{\eta_2}\sum_{m=1}^{3}\int_0^{K_{m,i}}\tilde{\rho}_{m,i}\big(\dot{\hat{\rho}}_{m,i}+\eta_2\Omega_{m,i}\mathcal{Z}(k,u_{m,i})\big)dk, \\ \mathcal{C}_{3,i} &= -\frac{1}{\eta_3}\tilde{d}_{i,\max}(\dot{\hat{d}}_{i,\max} - \eta_3\|\boldsymbol{\Omega}_i\|). \end{aligned}$$

According to (66), $\mathcal{C}_{1,i} = 0$ if $\|\hat{\boldsymbol{\chi}}_{\rho_0,i}\|^2 < \epsilon_{1,i}$ or if $\|\hat{\boldsymbol{\chi}}_{\rho_0,i}\|^2 \geq \epsilon_{1,i}$ and $\Upsilon_{1,i}^{\mathrm{T}}\hat{\boldsymbol{\chi}}_{\rho_0,i} < 0$. In addition, since when $\|\hat{\boldsymbol{\chi}}_{\rho_0,i}\|^2 \geq \epsilon_{1,i}$ and $\Upsilon_{1,i}^{\mathrm{T}}\hat{\boldsymbol{\chi}}_{\rho_0,i} \geq 0$, we can get

$$\mathcal{C}_{1,i}=\gamma_i\Big(\frac{(\|\hat{\boldsymbol{\chi}}_{\rho_0,i}\|^2-\epsilon_{1,i})\Upsilon_{1,i}^{\mathrm{T}}\hat{\boldsymbol{\chi}}_{\rho_0,i}}{\delta_{1,i}\|\hat{\boldsymbol{\chi}}_{\rho_0,i}\|^2}(\boldsymbol{\rho}_{0,i}\circ\tilde{\boldsymbol{\chi}}_{\rho_0,i})^{\mathrm{T}}\hat{\boldsymbol{\chi}}_{\rho_0,i}\Big)\leq 0,$$

which is true because $\tilde{\boldsymbol{\chi}}_{\rho_0,i}^{\mathrm{T}}\hat{\boldsymbol{\chi}}_{\rho_0,i} = \hat{\boldsymbol{\chi}}_{\rho_0,i}^{\mathrm{T}}\boldsymbol{\chi}_{\rho_0,i} - \|\hat{\boldsymbol{\chi}}_{\rho_0,i}\|^2 \leq 0$ when $\|\hat{\boldsymbol{\chi}}_{\rho_0,i}\|^2 \geq \epsilon_{1,i}$. Therefore, $\mathcal{C}_{1,i} \leq 0$. Similarly, we can obtain $\mathcal{C}_{2,i} \leq 0$ and $\mathcal{C}_{3,i} \leq 0$ by following the above analysis. Thus, $\dot{V}$ satisfies

$$\dot{V} \leq \sum_{i=1}^{N}\big(-k_1\Psi_i - (k_2-k_3)\|\boldsymbol{\Omega}_i\|\|\boldsymbol{e}_{\boldsymbol{\Omega},i}\|\big).$$

When the parameters $k_2 \geq k_3 > 0$ are configured, $\dot{V} \leq \sum_{i=1}^{N}\big(-k_1\Psi_i\big)$ can be further obtained.

Therefore, $\dot{V}$ is negative semi-definite. Then, by invoking the LaSalle-Yoshizawa theorem [34, Appendix A, Theorem A.8], it yields that $\lim_{t\to\infty}\Psi_i = 0$. Therefore, the system asymptotically converges to the minimum point $\boldsymbol{R}_i = \boldsymbol{R}_j = \boldsymbol{R}_d$ of Ψ_i while satisfies the mixed attitude constraints in the convergence process. When the system reaches the minimum point $\boldsymbol{R}_i = \boldsymbol{R}_j = \boldsymbol{R}_d$, $\dot{\boldsymbol{R}}_i = \dot{\boldsymbol{R}}_j = \dot{\boldsymbol{R}}_d$ is easy to get. Then, according to the attitude kinematics (2), $\lim_{t\to\infty}\boldsymbol{\Omega}_i = \boldsymbol{\Omega}_j = \boldsymbol{\Omega}_d$ is obtained.

In summary, $\lim_{t\to\infty}\boldsymbol{R}_i = \boldsymbol{R}_j = \boldsymbol{R}_d$ and $\lim_{t\to\infty}\boldsymbol{\Omega}_i = \boldsymbol{\Omega}_j = \boldsymbol{\Omega}_d$ means that while considering the mixed attitude constraints, input saturation and external disturbance, the attitude of the spacecraft in MSSs tends to be consistent, and track the time-varying desired attitude provided by the virtual leader spacecraft. This completes the proof. ■

REMARK 6. *Without considering the input saturation (6), the attitude dynamic of the i-th spacecraft in MSS is*

$$\boldsymbol{J}_i\dot{\boldsymbol{\Omega}}_i = -\boldsymbol{\Omega}_i\times\boldsymbol{J}_i\boldsymbol{\Omega}_i + \tilde{\boldsymbol{u}}_i + \boldsymbol{d}_i, \tag{70}$$

the adaptive controller can be designed as $\tilde{\boldsymbol{u}}_i = \boldsymbol{u}_i^0$, $\boldsymbol{u}_i^0$ is the virtual controller, which has been given in (65). Its stability can be proved by the following Lyapunov function without considering the input saturation of MSS

$$\begin{aligned} V' = \sum_{i=1}^{N}\big(&\frac{1}{2}\boldsymbol{\Omega}_i\boldsymbol{J}_i\boldsymbol{\Omega}_i + k_4V_{\boldsymbol{R},i} + V_{\boldsymbol{d}_{i,\max}} \\ &+ V_{\kappa_{1,i}} + V_{\kappa_{2,i}} + V_{\kappa_{3,i}} + V_{\kappa_{4,i}}\big). \end{aligned} \tag{71}$$

The proof process is similar to Theorem 1 and is omitted.

In other words, the proposed adaptive saturated controller (67) actually adopts the dead-zone based operation on the virtual controller $\boldsymbol{u}_i^0$ in (65). In addition, if the nonlinear saturation operation (6) is directly applied to $\boldsymbol{u}_i^0$ in (65), the actual torque input of the spacecraft can be obtained as ($m = 1, 2, 3$)

$$w_{m,i}=\mathrm{sat}(u_{m,i}^0)=\mathrm{sign}(u_{m,i}^0)\min(u_{\mathrm{sat},m,i},|u_{m,i}^0|). \tag{72}$$

The main difference between the proposed controller (67) and the controller (72) is that different input saturation operations are applied to the virtual controller $\boldsymbol{u}_i^0$ in (65). We will compare the two operations/controllers in the Simulation Results section.

REMARK 7. *Motived by [31], to implement controller (67), the integral term $\hat{h}_{m,i} = \int_0^{K_{m,i}}\hat{\rho}_{m,i}(k)\mathcal{Z}(k,u_{m,i})dk$ with $m = 1, 2, 3$, is approximated as:*

$$\int_0^{K_{m,i}}\hat{\rho}_{m,i}(k)\mathcal{Z}(k,u_{m,i})dk \simeq \sum_{s=1}^{M_{m,i}}\hat{\rho}_{m,i}(s\Delta k)\mathcal{Z}(s\Delta k,\boldsymbol{u}_{m,i})\Delta k. \tag{73}$$

Then, the corresponding $\dot{\hat{\rho}}_{m,i}(s\Delta k)$ becomes

$$\dot{\hat{\rho}}_{m,i}(s\Delta k) = \mathrm{Proj}\left(\hat{\rho}_{m,i}(s\Delta k), \bar{\Upsilon}_{2,i}\right), \tag{74}$$

with $\bar{\Upsilon}_{2,i}\triangleq\Omega_{m,i}\circ\mathcal{Z}(s\Delta k,u_{m,i})$, where Δk is a step size and $M_{m,i}=\frac{K_{m,i}}{\Delta k}$. Obviously, the smaller parameter Δk is selected, the more accurate the approximation is, but it will increase the computational complexity. The larger Δk, the larger the approximation error will be. Therefore, it is very important to select the value of parameter Δk.

REMARK 8. *Compared with the adaptive update law in [15], [31], we design the projection operator (62) to make the corresponding parameters closer to the actual physical value in the adaptive estimation process.*

REMARK 9. *The initial values of the adaptive parameters $\kappa_{1,i}(0)\neq 0$, $\kappa_{2,i}(0)\neq 0$, $\kappa_{3,i}(0)\neq 0$, $\kappa_{4,i}(0)\neq 0$ to prevent singularity. Taking advantages of $\kappa_{1,i}$, $\kappa_{2,i}$, $\kappa_{3,i}$, $\kappa_{4,i}$, the*

proposed controller (67) is a continuous controller, even though the sliding mode control method is used.

REMARK 10. *The proposed controller (67) can be degenerated into an attitude controller, which is suitable for a single spacecraft tracking system. As for the mixed potential function, only the terms related to the SFZ and the SMZ need to be considered, and the terms related to the DFZ are set to* 0*. Specifically, the proposed controller (67) for MSSs can be degenerated into a single spacecraft attitude tracking adaptive controller for spacecraft 1 as*

$$\bar{\boldsymbol{w}}_1 = \boldsymbol{\rho}_{0,1} \circ \hat{\boldsymbol{\chi}}_{\rho_0,1} \circ (\boldsymbol{u}_1^0 + \hat{\mathcal{H}}_1) - \mathcal{H}_1, \tag{75}$$

where

$$\begin{aligned} \boldsymbol{u}_1^0 = &- k_1 \Psi_1 \mathcal{S}_{1,1} - k_2 \|\boldsymbol{e}_{\boldsymbol{\Omega},1}\| \mathcal{S}_{2,1} - k_3 \boldsymbol{e}_{\boldsymbol{\Omega},1} \\ &- k_4 \mathcal{F}_1 + k_4 \mathcal{M}_1 \mathcal{S}_{3,1} - \hat{d}_{1,\max} \mathcal{S}_{4,1}, \end{aligned} \tag{76}$$

where $\Psi_1 = \Psi_{t,1}$, $\boldsymbol{e}_{\boldsymbol{\Omega},1} = \boldsymbol{e}_{\boldsymbol{\Omega},t,1}$, $\mathcal{F}_1 = \boldsymbol{e}_{\boldsymbol{R},1}\Phi_1 + \Psi_1(\mathcal{P}_{SF,1} + \mathcal{P}_{MF,1})$ *with* $\boldsymbol{e}_{\boldsymbol{R},1} = \boldsymbol{e}_{\boldsymbol{R},t,1}$, $\Phi_1 = 1 + \Phi_{SF,i} + \Phi_{SM,i}$, *and* $\mathcal{M}_1 = \Phi_1 \big(b_1 (\boldsymbol{R}_1^T \boldsymbol{R}_d \boldsymbol{\Omega}_d)^{\mathrm{T}} \boldsymbol{e}_{\boldsymbol{R},t,1}\big)$. *The definitions of other parameters are the same as those of the controller (67).*

VII. Simulation Results

In this section, the effectiveness of the proposed controller (67) is verified by numerical simulation of an MSS with mixed attitude constraints, input saturation and external disturbances.

We consider three spacecraft in the formation flying with a virtual leader providing a time-varying desired attitude $\boldsymbol{R}_d$. As shown in Fig. 3, in the directed complete communication topology, the virtual leader is only connected to the 1-st spacecraft in the MSS. In addition, the spacecraft in the MSS is assumed to have the same configuration. The inertia matrix of each spacecraft is

$$\boldsymbol{J}_i = \begin{bmatrix} 60 & 0 & -5 \\ 0 & 65 & 0 \\ -5 & 0 & 70 \end{bmatrix} \mathrm{kg \cdot m^2}, \ i = 1, 2, 3.$$

The external disturbance of each spacecraft is

$$\boldsymbol{d}_i = 10^{-3} \times \begin{bmatrix} -1 + 3\cos(0.1it) + 4\sin(0.03it) \\ 1.5 - 1.5\sin(0.02it) - 3\cos(0.05it) \\ 1 + \sin(0.1it) - 1.5\cos(0.04it) \end{bmatrix} \mathrm{N \cdot m},$$

where $i = 1, 2, 3$. The saturation limit of the actuators of the i-th spacecraft is given as $u_{\mathrm{sat},m,i} = 1$ N·m. Meanwhile, for the i-th spacecraft in the MSS, three spaceborne devices are equipped, including one sensitive spaceborne instrument (infrared telescope) to complete scientific observation, one communication spaceborne instrument (high gain antenna) to maintain ground communication, and three thrust engines to maintain the configuration of the MSS. The unit vectors $\boldsymbol{a}_i$, $\boldsymbol{b}_i$ and $\boldsymbol{h}_{k,i}$, $k = 1, 2, 3$ of the above three instruments installed the body-fixed frame $\mathcal{B}$ of the i-th spacecraft are $\boldsymbol{a}_i = [0, 0, 1]$, $\boldsymbol{b}_i = [0, 1, 0]$, $\boldsymbol{h}_{1,i} = [-1, 0, 0]$, $\boldsymbol{h}_{2,i} = [0, -1, 0]$, $\boldsymbol{h}_{3,i} = [0.750, 0.433, 0.500]$, respectively. The detailed information of the four static attitude-constrained zones in the inertial reference frame $\mathcal{I}$ is given in Table I. The constraint angle of relative Dynamic attitude-forbidden zone relating to center pointing vectors $h_{k,1}$, $h_{k,2}$, $h_{k,3}$ for the k-th thrust engine of three spacecraft is assumed to be 30 deg.

TABLE I
Parameters of static constrained-zones
(In the inertial reference frame $\mathcal{I}$)

Constrained zones	Center vector	Angle
Static Forbidden Zone 1 (SFZ1)	$[0, -1, 0]$	30 deg
Static Forbidden Zone 2 (SFZ2)	$[0.68, 0.67, 0.28]$	25 deg
Static Forbidden Zone 3 (SFZ3)	$[0.38, 0, 0.925]$	20 deg
Static Mandatory Zone 1 (SMZ1)	$[-0.813, 0.548, -0.192]$	50 deg

TABLE II
The initial states of the MSS

i	$\boldsymbol{R}_{i,0} = \exp(\theta_i, \boldsymbol{n}_i)$	$\boldsymbol{\Omega}_{i,0}$ rad/s
1	$\theta_1 = -80$ deg, $\boldsymbol{n}_1 = [0.2298, 0, -0.9732]$	$[0.03, 0.02, -0.03]$
2	$\theta_2 = -40$ deg, $\boldsymbol{n}_2 = [0, 0.7071, 0.7071]$	$[-0.02, 0.02, -0.03]$
3	$\theta_3 = -120$ deg, $\boldsymbol{n}_3 = [0.2298, 0, -0.9732]$	$[0, 0.03, 0.04]$

The initial states of the MSS are given in Table II, and the compliance of the initial attitude of the MSS with the mixed attitude constraints is shown in Table III, where we see that some attiude constraints are not satisfied initially. The parameter settings of the proposed adaptive saturation attitude continuous controller (67) and adaptive update law (66) of MSS are shown in Table IV.

In order to generate a reasonable time-varying desired attitude $\boldsymbol{R}_d$, the virtual leader spacecraft (spacecraft 0) is assumed to have a rest-to-rest maneuver in the absence of external disturbances but subject to static attitude constraints (SFZ1-3 and SMZ). The gains of the proposed controller $\boldsymbol{u}_{\boldsymbol{R}_d}$ are shown in Table IV and other parameters are the same as those in the MSS. In the simulation, the virtual leader spacecraft completes the attitude redirection from $\boldsymbol{R}_{0,0} = \exp(-0.9903, [0.2298, 0, -0.9732]^{\mathrm{T}})$ to $\boldsymbol{R}_{0,d} = \exp(-1.8546, [0.7030, -0.7112, 0]^{\mathrm{T}})$.

Next, we consider three numerical simulations to illustrate the overall performance of the proposed controller (67) and its ability to deal with input saturation.

A. Simulation Results of A Single Spacecraft Tracking

In this subsection, a single spacecraft attitude tracking system on $\mathrm{SO}(3)$ consisting of spacecraft 1 and the virtual leader spacecraft under attitude constraints, input saturation and external disturbances, is considered. Then, the performance of the degenerated attitude tracking adaptive controller (75) for spacecraft 1 subject to three attitude forbidden zones and one attitude mandatory zones given in Table III is evaluated.

The 2D projection in the inertial frame $\mathcal{I}$ of attitude trajectory of the single spacecraft tracking system using the degenerated attitude tracking adaptive controller (75) is shown in Fig. 4(a). It is obvious from Fig. 4(a) that the degenerated controller (75) realizes the tracking of the time-varying desired attitude, while the pointing directions of the amounted telescopes avoid the three

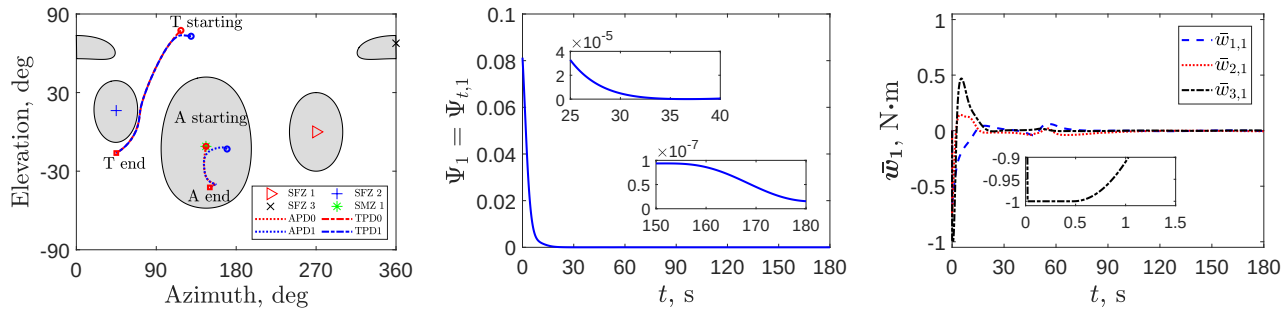

(a) 2D projection of attitude trajectory (b) Attitude tracking error (c) Actual torque

Fig. 4. The state time history of the single spacecraft tracking system with a time-varying rest-to-rest virtual leader under the degenerated controller (75). (A: antenna axis, T: telescope axis; APD0 and APD1: the desired antenna pointing direction (APD) of the virtual leader and the APD of Spacecraft 1; TPD0 and TPD1: the desired telescope pointing direction (TPD) of the virtual leader and the TPD of Spacecraft 1. The circle and the square are the starting point and the end point of the attitude movement, respectively.)

TABLE III

Satisfaction of initial attitude and mixed attitude constraints of the MSS (Y: satisfied, N: not satisfied)

i	SFZ 1	SFZ 2	SFZ 3	SMZ 1	$\boldsymbol{h}_{k,1}$	$\boldsymbol{h}_{k,2}$	$\boldsymbol{h}_{k,3}$
1	Y	Y	Y	Y	-	Y	Y
2	Y	N	Y	Y	Y	-	Y
3	Y	Y	Y	N	Y	Y	-

TABLE IV

Controller simulation parameters

Controller	Parameters
Proposed controller (67)	$k_1 = 0.01$, $k_2 = k_3 = 55$, $k_4 = 16$, $\mu_1 = \mu_2 = \mu_3 = 0.001$, $\mu_4 = 3$, $\kappa_{1,i}(0) = \kappa_{2,i}(0) = 0.05$, $\kappa_{3,i}(0) = \kappa_{4,i}(0) = 0.05$, $\alpha = \lambda = \beta = 0.05$, $\Delta r = 0.005$.
Virtual leader controller	$k_1 = 0.01$, $k_2 = k_3 = 30$, $k_4 = 0.2$.

SFZ, and the pointing direction of the antenna is always in the SMZ. Fig. 4(b) and Fig. 4(c) show the attitude tracking error and actual torque of the single spacecraft tracking system, respectively. We can observe that attitude tracking error converge to zero asymptotically and the actual control torque satisfies the saturation constraint.

In summary, the degenerated controller (75) can achieve the time-varying rest-to-rest attitude tracking of a single spacecraft tracking system on $\mathrm{SO}(3)$ under attitude constraints, input saturation and external disturbances.

B. Overall Simulation Results of MSSs

In this subsection, the overall performance of the proposed adaptive controller in (67) for the MSS on $\mathrm{SO}(3)$ with a time-varying rest-to-rest virtual leader under mixed attitude constraints, input saturation and external disturbances, is simulated.

The 2D projection in the inertial frame $\mathcal{I}$ of attitude trajectory of the MSS using the proposed controller (67) is shown in Fig. 5(a), where the red curve is the pointing trajectory of the two spaceborne instruments of the virtual leader spacecraft, and the other three colored curves represent the pointing trajectory of the two spaceborne instruments of the three following spacecraft in the MSS. It is obvious from Fig. 5(a) that the proposed controller (67) realizes the attitude consensus and the tracking of the time-varying desired attitude provided by the virtual leader of the MSS, while the pointing directions of the amounted telescopes avoid the three SFZ. It is also noted that the initial pointing direction of the telescope amount on the 2-nd spacecraft (i.e., TPD2) is within the SFZ3 and the initial pointing direction of the antenna of the 3-rd spacecraft (i.e., APD3) is outside the SMZ1. That is, the initial attitudes $\boldsymbol{R}_{2,0}$ and $\boldsymbol{R}_{3,0}$ violate attitude constraint (15) in the simulation. However, since the proposed controller (67) leverages the mixed potential function (15), it is observed from Fig. 5(a) that the attractive potential can make the TPD2 quickly leave SFZ3 and the APD3 quickly enter into SMZ1. Fig. 5(b)-5(d) show the attitude consensus error, attitude tracking error and angular velocity error of the MSS under the proposed controller (67), respectively. For the time-varying leader-follower MSS on $\mathrm{SO}(3)$, the proposed controller (67) can achieve attitude consensus and tracking of the time-varying desired attitude, where the attitude consensus is completed in 30 s with a steady-state error $\|\Psi_{c,i}\| \leq 1.5 \times 10^{-7}$ in 150 s, as shown in Fig. 5(b). The attitude tracking is completed in 45 s with a steady-state error $\|\Psi_{t,i}\| \leq 1.5 \times 10^{-6}$ in 150 s, as shown in Fig. 5(c). Based on the above results, the convergence rate of attitude consensus is faster than that of attitude tracking. Moreover, the angular velocity error, as shown in Fig. 5(d), tends to be stable in 90 s with a steady-state error $\|\boldsymbol{e}_{\boldsymbol{\Omega}_i}\| \leq 6 \times 10^{-3}$ deg/s in 150 s. In addition, it is noted that the attitude tracking error and the angular velocity error of spacecraft 1 are less than those of spacecraft 2 and spacecraft 3, but the attitude consensus error of spacecraft 1 is greater than that of spacecraft 2 and spacecraft 3. This is because spacecraft 1 is connected with the virtual leader and can directly obtain the desired attitude. Therefore, the adjustment of attitude tracking error of spacecraft 1 is faster than that of the other two spacecraft, whereas spacecraft 2 and

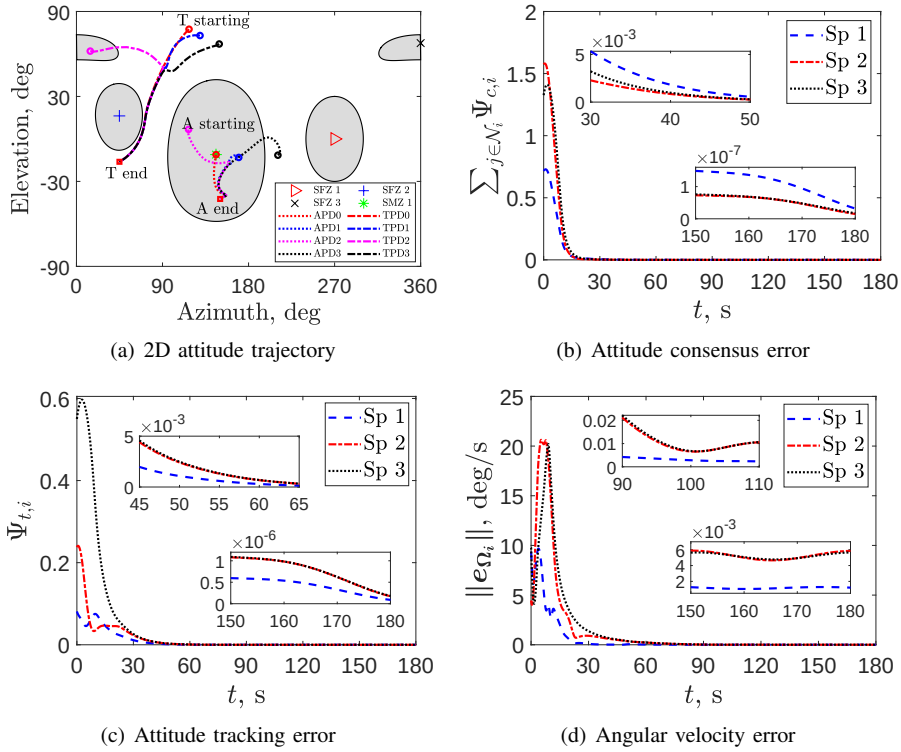

(a) 2D attitude trajectory

(b) Attitude consensus error

(c) Attitude tracking error

(d) Angular velocity error

Fig. 5. The state time history of the MSS under the proposed controller (67). (APD1-APD3: the antenna pointing direction (APD) of the three follower spacecraft. TPD1-TPD3: the telescope pointing direction (TPD) of the three follower spacecraft. Sp: spacecraft)

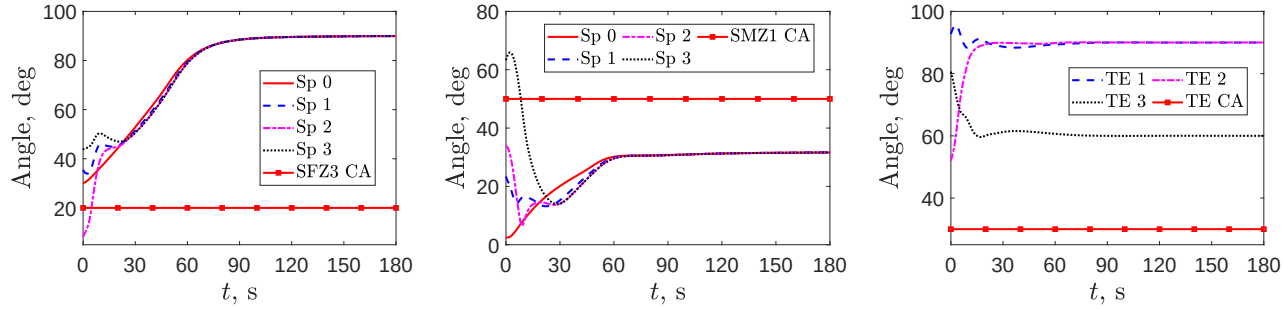

(a) Telescope axis and SFZ3

(b) Antenna axis and SMZ1

(c) Telescope axis of the 1-st Sp and three thrust engines of the 3-rd Sp

Fig. 6. The time history of the angle between the pointing of the spcaeborne equipment of each spacecraft and the central pointing of several attitude-constrainted zones. (SFZ3 CA: constraint angle of SFZ3, SMZ1 CA: constraint angle of SMZ1, TE CA: constraint angle of thrust engine)

spacecraft 3 only need to adjust the attitude consensus error to track the desired attitude. In addition, it can be seen from Fig. 4(b) that the single spacecraft can track the desired attitude in 30 s, while for the MSSs can track the desired attitude in 55 s from Fig. 5(c). This is because the attitude consensus of spacecraft is considered in the MSSs, and the desired attitude tracking can be completed only after the consensus of the MSSs is achieved.

The angle between the pointing of the spaceborne equipment of each spacecraft and the central pointing of several attitude-constrained zones in the MSS is shown in Fig. 6. It can be seen that the telescope axis of spacecraft 2 initially points inside SFZ3 and the antenna axis of spacecraft 3 initially points outside SMZ1. Since the proposed potential function (40) considers arbitrary initial attitude of the spacecraft, the spacecraft quickly reaches the state that meets the attitude constraints. In addition, from Fig. 6(c), the relative dynamic attitude constraint is always satisfied. Compared with the previous potential functions in [25]–[27], the proposed one in (40) is effective for arbitrarily initial attitude of the spacecraft. Fig. 7 shows the actual torque of each spacecraft in the MSS with a time-varying rest-to-rest virtual leader under the proposed controller (67). It is obvious that the actual torque of each spacecraft meets the input saturation.

In summary, the proposed controller (67) with the adaptive update law (66) can achieve attitude consensus and the time-varying rest-to-rest attitude tracking of MSS on $\mathrm{SO}(3)$ under arbitrary initial attitude, mixed attitude constraints, input saturation and external disturbances.

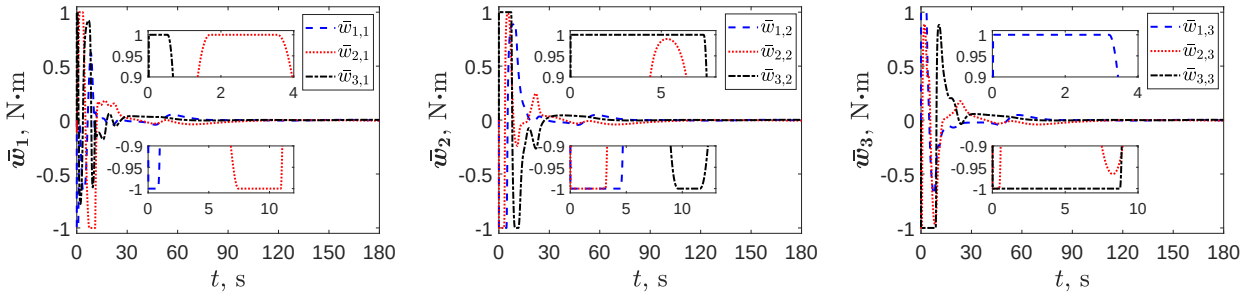

(a) Spacecraft 1 (b) Spacecraft 2 (c) Spacecraft 3

Fig. 7. The time history of actual torque of each spacecraft in the MSS under the proposed controller (67).

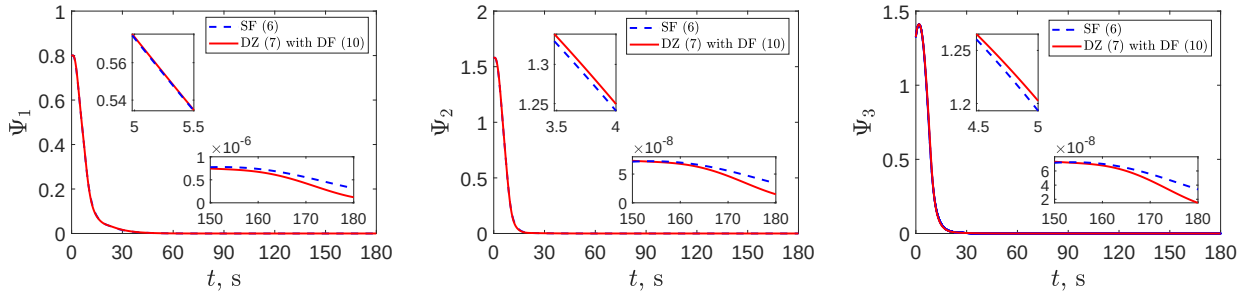

(a) Spacecraft 1 (b) Spacecraft 2 (c) Spacecraft 3

Fig. 8. Comparison of the attitude error time history of each spacecraft in the MSS under different input saturation operations.

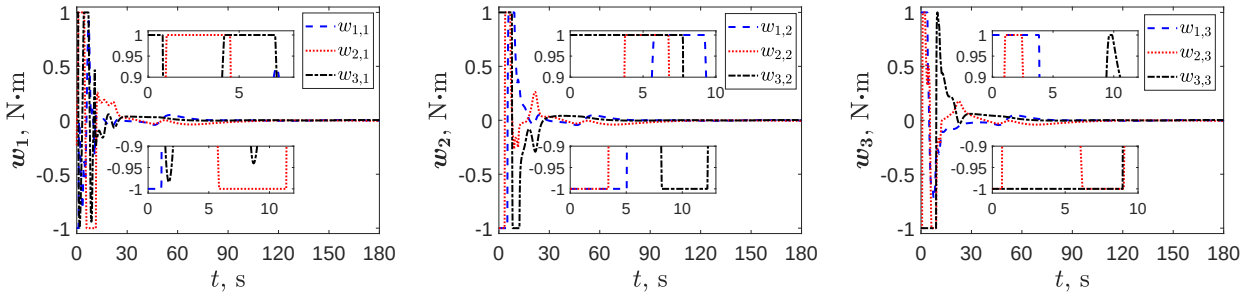

(a) Spacecraft 1 (b) Spacecraft 2 (c) Spacecraft 3

Fig. 9. The time history of actual torque of each spacecraft in the MSS under the controller (72) with saturation function (6).

C. Different Input Saturation Operations

In this subsection, we show the advantages of the input saturation model under the dead-zone operation (7). The following two input saturation operations are simulated:

1) Operation 1 [SF (6)]: The saturation function (6) is directly applied to the virtual controller (65), i.e., the saturated controller (72).
2) Operation 2 [DZ (7) with DF (10)]: The dead-zone operation (7) under density function (10) is applied to the virtual controller (65), i.e., the proposed saturated controller (67).

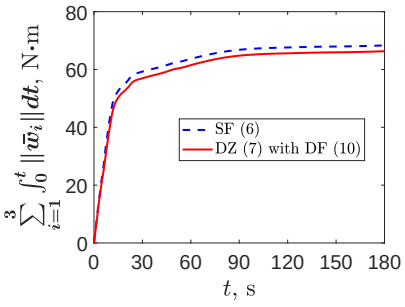

Fig. 10. Energy consumption of different input saturation operations.

To obtain a fair comparison, the parameters of the two operations are set to the same, as shown in Table IV. Fig. 8 shows the attitude error Ψ_i of each spacecraft in MSS under two input saturation operations. The attitude error convergence speed of operation 2 is slower than that of Operation 1 in the initial stage, but its convergence accuracy is higher than Operation 1. From Fig. 9 and previous result in Fig. 7, the saturation duration of the operation 2 is significantly reduced compared with the operation 1. To elaborate this, we count the total saturation duration

of all attitude actuators under two operations. The total saturation duration under Operation 1 is 58.56 s, while operation 2 has 36.02 s, indicating that the saturation duration under Operation 2 decreases by 38.49% compared with operation 1. Meanwhile, when the actuators exit the saturation, the dead-zone based operation has a relatively gentle and soft transition without sharp changes of control inputs. In addition, we also use $\sum_{i=1}^{3}\int_0^T \|\bar{\boldsymbol{w}}_i\|dt$ to represent the energy consumption of the MSS, where T is the total maneuvering time. As shown in Fig. 10, the operation 2 consumes less energy than Operation 1, which is consistent with the theoretical analysis in Remark 1.

Through the above analysis, the proposed adaptive saturated attitude controller (67) using the dead-zone operation (7) can approximate the nonlinear saturation on the premise of ensuring the stability of the MSS. Meanwhile, the dead-zone operation (7) under density function (10) reduces the saturation duration significantly.

VIII. Conclusions

In this paper, an adaptive attitude controller of the leader-follower MSS on $\mathrm{SO}(3)$ is proposed to realize attitude consensus and attitude tracking with arbitrary initial attitude under mixed attitude constraints, saturation constraints and external disturbances. Considering the time-varying desired attitude provided by the virtual leader, attitude error function and dynamics are developed for MSS on $\mathrm{SO}(3)$ under a directed complete communication topology. Next, a mixed potential function on $\mathrm{SO}(3)$ is proposed for the static attitude-forbidden zones, the relative dynamic attitude-forbidden zones and the attitude-mandatory zones, although the MSS may have arbitrary initial attitude. An adaptive saturated controller is designed to realize attitude consensus and tracking, while satisfying mixed attitude constraints and saturation constraints. Finally, simulation results demonstrate that the proposed controller achieves attitude consensus and the time-varying desired attitude tracking of MSS on $\mathrm{SO}(3)$ with arbitrary initial attitudes. In future works, to obtain the optimal control performance for constrained MSSs, the application of nonlinear model predictive control for MSSs on $\mathrm{SO}(3)$ will be explored.

REFERENCES

[1] R. W. Beard, J. Lawton, and F. Y. Hadaegh, "A coordination architecture for spacecraft formation control," *IEEE Transactions on Control Systems Technology*, vol. 9, no. 6, pp. 777–790, 2001, doi:10.1109/87.960341.

[2] D. Lee, A. K. Sanyal, and E. A. Butcher, "Asymptotic tracking control for spacecraft formation flying with decentralized collision avoidance," *Journal of Guidance, Control, and Dynamics*, vol. 38, no. 4, pp. 587–600, 2015, doi:10.2514/1.G000101.

[3] C. Wei, J. Luo, H. Dai, and G. Duan, "Learning-based adaptive attitude control of spacecraft formation with guaranteed prescribed performance," *IEEE Transactions on Cybernetics*, vol. 49, no. 11, pp. 4004–4016, 2018, doi:10.1109/TCYB.2018.2857400.

[4] N. A. Chaturvedi, A. K. Sanyal, and N. H. McClamroch, "Rigid-body attitude control," *IEEE Control Systems Magazine*, vol. 31, no. 3, pp. 30–51, 2011, doi:10.1109/MCS.2011.940459.

[5] J. Stuelpnagel, "On the parametrization of the three-dimensional rotation group," *SIAM review*, vol. 6, no. 4, pp. 422–430, 1964, doi:10.1137/1006093.

[6] Y. Guo, S.-M. Song, and X.-H. Li, "Finite-time output feedback attitude coordination control for formation flying spacecraft without unwinding," *Acta Astronautica*, vol. 122, pp. 159–174, 2016, doi:10.1016/j.actaastro.2016.01.015.

[7] T. Lee, "Global exponential attitude tracking controls on SO(3)," *IEEE Transactions on Automatic Control*, vol. 60, no. 10, pp. 2837–2842, 2015, doi:10.1109/TAC.2015.2407452.

[8] S. Kulumani, C. Poole, and T. Lee, "Geometric adaptive control of attitude dynamics on SO(3) with state inequality constraints," in *2016 American Control Conference (ACC)*. Boston, MA, July 6-8, USA, 2016, pp. 4936–4941, doi:10.1109/ACC.2016.7526135.

[9] H. Du, M. Z. Chen, and G. Wen, "Leader–following attitude consensus for spacecraft formation with rigid and flexible spacecraft," *Journal of Guidance, Control, and Dynamics*, vol. 39, no. 4, pp. 944–951, 2016, doi:10.2514/1.G001273.

[10] Y. Liu, P. Huang, F. Zhang, and Y. Zhao, "Distributed formation control using artificial potentials and neural network for constrained multiagent systems," *IEEE Transactions on Control Systems Technology*, vol. 28, no. 2, pp. 697–704, 2018, doi:10.1109/TCST.2018.2884226.

[11] T. Chen, J. Shan, and H. Wen, "Distributed adaptive attitude control for networked underactuated flexible spacecraft," *IEEE Transactions on Aerospace and Electronic Systems*, vol. 55, no. 1, pp. 215–225, 2018, doi:10.1109/TAES.2018.2849904.

[12] J. Li, S. Chen, C. Li, and F. Wang, "Distributed game strategy for formation flying of multiple spacecraft with disturbance rejection," *IEEE Transactions on Aerospace and Electronic Systems*, vol. 57, no. 1, pp. 119–128, 2020, doi:10.1109/TAES.2020.3010593.

[13] H. Rezaee and F. Abdollahi, "Robust attitude alignment in multispacecraft systems with stochastic links failure," *Automatica*, vol. 118, p. 109033, 2020, doi:10.1016/j.automatica.2020.109033.

[14] Q. Wang and C.-Y. Su, "Robust adaptive control of a class of nonlinear systems including actuator hysteresis with prandtl–ishlinskii presentations," *Automatica*, vol. 42, no. 5, pp. 859–867, 2006, doi:10.1016/j.automatica.2006.01.018.

[15] S. H. Mousavi and A. Khayatian, "Dead-zone model based adaptive backstepping control for a class of uncertain saturated systems," *Asian Journal of Control*, vol. 18, no. 4, pp. 1395–1405, 2016, doi:10.1002/asjc.1198.

[16] M. Chen, P. Shi, and C.-C. Lim, "Robust constrained control for mimo nonlinear systems based on disturbance observer," *IEEE Transactions on Automatic Control*, vol. 60, no. 12, pp. 3281–3286, 2015, doi:10.1109/TAC.2015.2450891.

[17] X. Yan, M. Chen, Q. Wu, and S. Shao, "Dynamic surface control for a class of stochastic non-linear systems with input saturation," *IET Control Theory & Applications*, vol. 10, no. 1, pp. 35–43, 2015, doi:10.1049/iet-cta.2015.0031.

[18] C. Zhu, E. Zhang, J. Li, B. Huang, and Y. Su, "Approximation-free appointed-time tracking control for marine surface vessel with actuator faults and input saturation," *Ocean Engineering*, vol. 245, p. 110468, 2022, doi:10.1016/j.oceaneng.2021.110468.

[19] Z. Yin, J. Luo, and C. Wei, "Novel adaptive saturated attitude tracking control of rigid spacecraft with guaranteed transient and steady-state performance," *Journal of Aerospace Engineering*, vol. 31, no. 5, p. 04018062, 2018, doi:10.1061/(ASCE)AS.1943-5525.0000884.

[20] U. Lee and M. Mesbahi, "Feedback control for spacecraft reorientation under attitude constraints via convex potentials," *IEEE Transactions on Aerospace and Electronic Systems*, vol. 50, no. 4, pp. 2578–2592, 2014, doi:10.1109/TAES.2014.120240.

[21] E. L. de Angelis, F. Giulietti, and G. Avanzini, "Single-axis pointing of underactuated spacecraft in the presence of path constraints," *Journal of Guidance, Control, and Dynamics*, vol. 38, no. 1, pp. 143–147, 2015, doi:10.2514/1.G000121.

[22] X. Tan, S. Berkane, and D. V. Dimarogonas, "Constrained attitude maneuvers on SO(3): Rotation space sampling, planning and low-level control," *Automatica*, vol. 112, p. 108659, 2020, doi:10.1016/j.automatica.2019.108659.

[23] D. Y. Lee, R. Gupta, U. V. Kalabić, S. Di Cairano, A. M. Bloch, J. W. Cutler, and I. V. Kolmanovsky, "Constrained attitude maneuvering of a spacecraft with reaction wheel assembly by nonlinear model predictive control," in *2016 American Control Conference (ACC)*. IEEE, 2016, pp. 4960–4965, doi:10.1109/ACC.2016.7526139.

[24] D. Y. Lee, R. Gupta, U. V. Kalabić, S. Di Cairano, A. M. Bloch, J. W. Cutler, and I. V. Kolmanovsky, "Geometric mechanics based nonlinear model predictive spacecraft attitude control with reaction wheels," *Journal of Guidance, Control, and Dynamics*, vol. 40, no. 2, pp. 309–319, 2017, doi:10.2514/1.G001923.

[25] Q. Shen, C. Yue, C. H. Goh, B. Wu, and D. Wang, "Rigid-body attitude stabilization with attitude and angular rate constraints," *Automatica*, vol. 90, pp. 157–163, 2018, doi:10.1016/j.automatica.2017.12.029.

[26] Q. Hu, Y. Liu, H. Dong, and Y. Zhang, "Saturated attitude control for rigid spacecraft under attitude constraints," *Journal of Guidance, Control, and Dynamics*, vol. 43, no. 4, pp. 790–805, 2020, doi:10.2514/1.G004613.

[27] T. Chen and J. Shan, "Distributed spacecraft attitude tracking and synchronization under directed graphs," *Aerospace Science and Technology*, vol. 109, p. 106432, 2021, doi:10.1016/j.ast.2020.106432.

[28] C. Zhang, J. Wang, D. Zhang, and X. Shao, "Fault-tolerant adaptive finite-time attitude synchronization and tracking control for multi-spacecraft formation," *Aerospace Science and Technology*, vol. 73, pp. 197–209, 2018, doi:10.1016/j.ast.2017.12.004.

[29] S. Berkane, A. Abdessameud, and A. Tayebi, "Hybrid global exponential stabilization on SO(3)," *Automatica*, vol. 81, pp. 279–285, 2017, doi:10.1016/j.automatica.2017.04.001.

[30] T. Lee, "Exponential stability of an attitude tracking control system on SO(3) for large-angle rotational maneuvers," *Systems & Control Letters*, vol. 61, no. 1, pp. 231–237, 2012, doi:10.1016/j.sysconle.2011.10.017.

[31] S. H. Mousavi and A. Khayatian, "Dead zone model based adaptive backstepping control for a class of uncertain saturated systems," *IFAC Proceedings Volumes*, vol. 44, no. 1, pp. 14 489–14 494, 2011, doi:10.3182/20110828-6-IT-1002.00953.

[32] R. A. Horn, "The hadamard product," in *Proceedings of Symposia in Applied Mathematics*, vol. 40, 1990, p. 88.

[33] D. Thakur, S. Srikant, and M. R. Akella, "Adaptive attitude-tracking control of spacecraft with uncertain time-varying inertia parameters," *Journal of guidance, control, and dynamics*, vol. 38, no. 1, pp. 41–52, 2015, doi:514/1.G000457.

[34] M. Krstic, P. V. Kokotovic, and I. Kanellakopoulos, *Nonlinear and adaptive control design*. John Wiley and Sons, Inc., 1995, ch. Appendix A, p. 492.

Zeyu Kang was born in Shaanxi, China, in 1994. He received the B.E. and M.E. degrees in control science and engineering from Northwestern Polytechnical University, Xi'an, China, in 2016 and 2019, respectively.

He is currently working toward a Ph.D. degree from the school of Aeronautics and Astronautics, Shanghai Jiao Tong University, Shanghai, China. His research interests include spacecraft control under multiple constraints.

Qiang Shen (Member, IEEE) received his B.E. degree in automation from the Northwestern Polytechnical University, Xi'an, China, in 2010 and the Ph.D. degree from Nanyang Technological University, Singapore, in 2016.

From 2015 to 2017, he held a Research Scientist position at Temasek Laboratories, National University of Singapore, Singapore. From 2017 to 2019, he was a Postdoctoral Research Associate with the Mechanical and Aerospace engineering, Arizona State University, Tempe, AZ, USA. Currently, he is an Associate Professor in the School of Aeronautics and Astronautics, Shanghai Jiao Tong University, China. His research interests include spacecraft dynamics and control, fault diagnosis and tolerant control, active model discrimination, and control allocation.

Shufan Wu was born in China in 1964. He received the B.E., M.E., and Ph.D. degrees from Nanjing University of Aeronautics and Astronautics, Nanjing, China, in 1984, 1987, and 1990, respectively.

He was a research fellow with Surrey Space Centre UK, TU Delft, Netherlands TU Braunschweig Germany from 1995 to 2002. He was a Senior Engineer with European Space Technology and Research Center (ESTEC), ESA, from 2002 to 2013. Since 2017, he has been with the school of Aeronautics and Astronautics, Shanghai Jiao Tong University (SAA SJTU) and is currently an Executive Dean and Chair Professor of SAA SJTU. His current research interests include navigation guidance and control and intelligent micro-satellite technology and application.

Prof. Wu is a Corresponding Member of the International Academy of Astronautics and an Associate Fellow of the American Institute of Aeronautics and Astronautics.

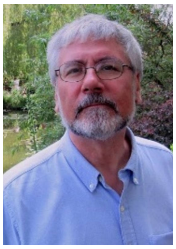

Christopher J. Damaren was born in Toronto, ON, Canada, in 1962. He received the B.A.Sc. degree in engineering science from the University of Toronto, Toronto, in 1985, and the M.A.Sc. and Ph.D. degrees in aerospace engineering from the University of Toronto Institute for Aerospace Studies (UTIAS), North York, ON, Canada, in 1987 and 1990, respectively.

He was an Assistant Professor with the Department of Engineering, Royal Roads Military College, Victoria, BC, Canada, from 1990 to 1995. From 1995 to 1999, he was a Senior Lecturer with the Department of Mechanical Engineering, University of Canterbury, Christchurch, New Zealand. Since 1999, he has been with UTIAS and is currently a Director and Professor of UTIAS. His current research interests include dynamics and control of space systems.

Prof. Damaren is a Fellow of the Canadian Aeronautics and Space Institute and an Associate Fellow of the American Institute of Aeronautics and Astronautics.